AIMS Mathematics, 10(4): 8721–8752.
DOI: 10.3934/math.2025400
Received: 30 January 2025
Revised: 26 March 2025
Accepted: 02 April 2025
Published: 15 April 2025

https://www.aimspress.com/journal/Math

Research article

Analytical soliton solutions of the Kairat-II equation using the Kumar–Malik and extended hyperbolic function methods

Abdul Mateen[1,*], **Ghulam Hussain Tipu**[2,3], **Loredana Ciurdariu**[4,*] **and Fengping Yao**[2,3]

[1] Ministry of Education Key Laboratory for NSLSCS, School of Mathematical Sciences, Nanjing Normal University, Nanjing, 210023, China

[2] Department of Mathematics, Shanghai University, No. 99 Shangda Road, Shanghai 200444, China

[3] Newtouch Center for Mathematics of Shanghai University, Shanghai 200444, China

[4] Department of Mathematics, Politehnica University of Timișoara, 300006 Timișoara, Romania

* **Correspondence:** Email: aabdulmateen1996@gmail.com; loredana.ciurdariu@upt.ro.

Abstract: The study of optical solitons has advanced significantly due to their stability and diverse applications, particularly in high-speed telecommunications, optical signal processing, and quantum technologies. This paper focuses on the derivation of exact soliton solutions for the nonlinear Kairat-II (K-II) equation, which models second-order spatiotemporal and group velocity dispersion effects in nonlinear optical systems. By applying the Kumar–Malik method and the extended hyperbolic function method, a comprehensive set of soliton solutions are obtained, capturing the intricate propagation dynamics of solitons in nonlinear media. The Kumar–Malik method yields numerous soliton solutions such as Jacobi elliptic function solution with an elliptic modulus, the trigonometric function solution, the hyper-trigonometric solution, dark solitons, bright solitons, periodic, singular and rational function solutions, etc. The behavior, stability, and evolution of these solitons are further illustrated through two-dimensional (2D), three-dimensional (3D), and contour plots, providing insights into their structural characteristics under various physical conditions. In this article, new soliton solutions in Jacobi elliptic form are derived for the given equation, providing valuable insights into the theoretical framework of solitons in nonlinear optics and presenting potential advancements for soliton-based technologies.

Keywords: Kairat-II equation; Kumar–Malik method; extended hyperbolic function method; Jacobi elliptic function; traveling wave solutions
Mathematics Subject Classification: 35Q51, 35C08, 35C07, 35A20

1. Introduction

Recently, nonlinear partial differential equations (PDEs) has become enormously important in pure and applied mathematics [1]. Advancements in computational technology have opened a new realm to researchers in the applied sciences [2], and this trend is largely attributable to such developments in computational technology. The common occurrence of nonlinear PDEs as mathematical models of complex phenomena has led to the essentially relevant nature of nonlinear PDEs in disciplines like engineering and mathematical physics [3]. Now as these fields are becoming more and more based on computational methods, understanding the theory of nonlinear PDEs becomes important. Nonlinear PDEs play a vital role in modern scientific inquiry, as they have solid mathematical backing and ample power from modern computing capabilities [4].

Optical solitons in nonlinear materials are a particular area of focus, namely wave packets, which can retain their properties over a large distance. This article shows the important role these equations play in the fields of science and in practical applications. For example, optical solitons' preservation of their integrity is essential for high-speed data transmission in optical fibers and the functionality of all optical switches [5]. To enable reliable and effective utilization of modern telecommunications, it is critical to understand this property, which explains the intense interest in optimizing optical solitons for these uses. In particular, the exploration of nonlinear PDEs and optical solitons [6] clearly demonstrates that mathematics and computer technology play an extremely important role in modern scientific progress, especially in application-related activities and technological innovations [7]. Nonlinear PDEs are critical for representing a wide range of complex physical phenomena where the relationship among variables is nonlinear and interactions are complex [8, 9]. Extensive applications of this timeseries can be found in plasma physics [10], fiber optics [11, 12], mathematical physics, telecommunication engineering, and optics. Therefore, nonlinear PDEs offer critical insights about the intricate dynamics of these systems in these fields [13], which enhances progress in both research and technology. As a result, they are essential for studying and modeling many complex, real world processes. In [14], Tipu et al. introduced optical soliton wave solutions of the non-linear Kairat-X equation via a new expanded direct algebraic method. Li et al. [15] studied Riemann–Hilbert problem and interactions of solitons in three component nonlinear Schrödinger equations.

Analytical methods have been widely employed to solve nonlinear partial differential equations (NLPDEs). Some commonly used approaches in the literature include the extended hyperbolic function method [16], The RB Sub-ODE (Reduced Basis Sub-Ordinary Differential Equation) approach, and the generalized tanh-coth method [17, 18]. Other frequently utilized techniques are the improved $tan(\phi^2)$-expansion technique [19] and the formal linearization approach [20–24], which have been applied to derive soliton solutions. Furthermore, bi-Hamiltonian systems of multi-component integrable derivative nonlinear Schrödinger models [25] have been developed from specific matrix spectral problems. In [26], the author provided multi-soliton solutions, and breather-like and bound-state solitons for the complex modified Korteweg–de Vries equation in optical fibers. Nasreen et al. [27, 28] explored exact solutions for various nonlinear models using different analytical techniques. Another study [29] explored solitary wave solutions to a fractional model using the improved modified extended *tanh*-function method. However, soliton dynamics in dispersive NLSE systems have been extensively studied, with notable contributions from Samir et al. [31], who utilized the improved modified extended tanh function method to analyze the nonlinearity

described by Kudryashov's law. Additionally, Ismael et al. [30] investigated the Nizhnik–Novikov–Veselov equation, examining the phenomenon of wave interactions. Dynamic systems include research on both chaotic and periodic orbits; bifurcations denote critical parameter values at which the system's behavior suddenly changes. These changes can either enhance or reduce the system's stability. Methods such as virtual simulations, iterative mapping, and differential equations help analyze these dynamics. Key analytical tools include time series analysis, phase space diagrams, Poincaré sections, Lyapunov exponents, and bifurcation diagrams, all of which provide insights into a system's evolution, periodicity, and chaotic behavior; for more details, one can consult [32–38] and the references therein. Recently, scientists, led by Yang [39], have initiated a profound journey into the realm of ferroelectric materials to unveil insight into ultra-high piezoelectricity. In [40], the researchers studied this equation in depth, discovering kink solitons and periodic wave solutions. Wang et al. [41] addressed gaps in the literature by introducing various solitons with fractional operators. Similarly, [42,43] introduced bright solitons using the extended tanh technique and the direct extended algebraic approach. This work aims to fill these gaps using novel techniques and provides additional insight into wave propagation and the effect of new parameters.

We consider the following Kairat-II equation (K-IIE) [44]:

$$\mu_{\varkappa\tau} - 2\mu_{\tau}\mu_{\varkappa\varkappa} - 4\mu_{\varkappa}\mu_{\varkappa\tau} + \mu_{\varkappa\varkappa\varkappa\tau} = 0. \tag{1.1}$$

The system comprises interconnected nonlinear partial differential equations. The real wave function, $\mu(\varkappa, \tau)$ varies across both space ($\varkappa$) and time (τ), reflecting the system's behavior over these dimensions.

The importance of solitons in optical applications, particularly in fiber optics, is well-established due to their stability and ability to propagate over long distances without distortion. Among various soliton models, the Kairat-II (K-II) equation has attracted significant attention for its capacity to describe complex nonlinear wave phenomena, such as pulse propagation in optical fibers. As an extension of the classical Korteweg–de Vries (KdV) equation, the K-II equation accounts for additional nonlinearities and dispersion effects, making it a more accurate model for real-world optical systems. This equation plays a crucial role in applications such as pulse shaping, optical communication, and energy transfer in nonlinear media. Compared with simpler models like the standard KdV equation or the modified Korteweg–de Vries (mKdV) equation, the K-II equation offers a more comprehensive framework by incorporating higher-order nonlinearities and dispersion, allowing for more precise descriptions of wave dynamics in optical fibers. By comparing the K-II equation with other models, we can better understand its advantages and potential limitations, offering a deeper insight into its significance for modern research in nonlinear optics.

This work explores complex structures across various fields, providing key insights into system dynamics, stability, and behavior. It uniquely examines nonlinear dynamical equations, independent of the Kairat-II equation, yet relevant to multiple physical scenarios. Building on previous advancements, this study employs Kumar–Malik and the extended hyperbolic function method, which offers a versatile approach to determine both general and specific solutions, including solitary wave solutions such as the Jacobi elliptic function solution with an elliptic modulus, the trigonometric function solution, the hyper-trigonometric solution, dark solitons, bright solitons, and periodic, singular, and rational function solution, etc. These solutions are visualized through two-dimensional (2D) and three-dimensional (3D) plots and contour diagrams to reflect the relevant constraints accurately. This visualization ensures that the results are presented clearly and effectively, incorporating realistic parameters. The findings from

this analysis not only enhance our comprehension of the dynamics but also offer valuable insights for modeling and designing future technical improvements. Indeed, this research will seek to close the gap in translation of theoretical developments in physics and engineering and applied mathematics into practice.

The Kumar–Malik method is particularly well-suited for the K-II equation due to its ability to systematically generate a wide range of exact solutions by reducing the equation into solvable forms. While this approach efficiently captures various soliton structures, its applicability is primarily limited to equations that can be transformed accordingly. Similarly, the extended hyperbolic function method provides additional solution families but is constrained by its dependence on hyperbolic nonlinearities. A discussion of the strengths and limitations of these methods is presented, offering insights into their suitability for solving the K-II equation. However, the soliton solutions obtained in this study have significant implications for various soliton-based technologies, including optical fiber communication, plasma physics, and nonlinear wave dynamics. In optical fiber systems, solitons play a crucial role in maintaining stable signal transmission over long distances with minimal dispersion, making the derived solutions valuable for improving fiber optic communication models. Similarly, in plasma physics, these solutions contribute to the understanding of nonlinear wave interactions, which are essential in designing advanced plasma confinement systems. Furtermore, solitons' behavior in fluid mechanics and Bose–Einstein condensates further highlights the relevance of these findings.

The structure of the paper is as follows. Section 2 presents the fundamental algorithms associated with the methods, which are further subdivided into Subsections 2.1 and 2.2, detailing the Kumar–Malik method and the extended hyperbolic function technique, respectively. In Section 3, we derive exact solutions for the nonlinear Kairat-II equation utilizing the aforementioned techniques. Section 4 presents results and discussion. The paper culminates in Section 5.

2. Description of the method

In this section, we outline the two analytical approaches utilized to solve the Kairat-II equation. Consider the following nonlinear evolution equation for $\mu(\varkappa, \tau)$:

$$\Pi(\mu, \mu_{\varkappa}, \mu_{\tau}, \mu_{\varkappa\varkappa}, \mu_{\varkappa\varkappa}, \mu_{\tau\tau}, ...) = 0, \tag{2.1}$$

where Π is a polynomial of $\mu(\varkappa, \tau)$. We also use the wave transformation technique

$$\mu(\varkappa, \tau) = \Upsilon(\eta), \ \eta = \omega(\varkappa - \lambda\tau). \tag{2.2}$$

Here, with λ as a constant, Eq (2.1) can be reformulated as the following nonlinear ordinary differential equation:

$$\Lambda(\Upsilon, \Upsilon', \Upsilon'', \Upsilon''', \Upsilon'''', ...) = 0. \tag{2.3}$$

The powers of Υ denote differentiation with respect to η.

Wave transmission techniques are essential for understanding and analyzing the propagation of waves, such as sound, electromagnetic, and mechanical waves, through various media. These techniques, widely applied in fields such as physics, engineering, and telecommunications, encompass methods like transmission line theory, Fourier analysis, and waveguides to study how waves transmit energy and information. Recent advancements have highlighted improvements in wave transmission through random media, where symmetry has been shown to enhance transmitted intensity [48]. Such techniques play a significant role in modern communication, imaging, and geophysical applications.

2.1. The Kumar–Malik method

The Kumar–Malik method serves as an analytical approach for addressing nonlinear partial differential equations, proving especially advantageous in situations characterized by nonlinear behavior. For further details on the Kumar–Malik method, see [45–47]. These studies collectively enhance the theoretical and practical understanding of nonlinear wave models across diverse scientific fields. Let us assume that the solution for Eq (2.3) can be expressed in the following form:

$$\Upsilon(\eta) = \Xi_0 + \Xi_1 F(\eta) + \Xi_2 F(\eta)^2 + ... + \Xi_N F(\eta)^N = \sum_{i=0}^{N} \Xi_i F(\eta)^i. \tag{2.4}$$

The constants Ξ_i (where $i = 1, 2, \ldots, N$) remain to be determined, and the function $F(\eta)$ satisfies the following first-order ordinary differential equation:

$$F'(\eta) = \sqrt{\sigma_1 F(\eta)^4 + \sigma_2 F(\eta)^3 + \sigma_3 F(\eta)^2 + \sigma_4 F(\eta) + \sigma_5}, \tag{2.5}$$

where $\sigma_j' s (j = 1, 2, 3, 4, 5)$ are arbitrary constants.

To ascertain N in Eq (2.4), we employ balancing methods, equating the highest-order derivative with the nonlinear term of the highest degree to establish equilibrium within the equation.

Substituting Eq (2.4) and its derivatives, as defined in Eq (2.5), into Eq (2.3) results in a polynomial in $F(\eta)F^{'}(\eta)$. By gathering all coefficients of the various powers and setting them to zero, we derive a system of equations that involves the unknown parameters λ, $\Xi_i' s (i = 1, 2, ..., N)$ and $\sigma_j' s (j = 1, 2, 3, 4, 5)$. Solving this system yields the exact solutions to Eq (2.3). By applying these solutions in conjunction with the transformation specified in Eq (2.2), we can obtain multiple exact solutions for the NLPDE represented by Eq (2.1).

Solutions of Eq (2.5)

Case 1. When $\sigma_4 = \frac{\sigma_2(4\sigma_1\sigma_3 - \sigma_2^2)}{8\sigma_1^2}$, $\sigma_5 = 0$. Consequently, Eq (2.5) possesses the following Jacobi elliptic solutions:

Subcase 1.1. If $\sigma_1 < 0,\ (4\sigma_1\sigma_3 - \sigma_2^2) > 0$, then

$$F_1(\eta) = -\frac{\sigma_2}{4\sigma_1} \pm \frac{\sigma_2}{4\sigma_1}\, cn\left(\frac{\sqrt{-\sigma_1(4\sigma_1\sigma_3 - \sigma_2^2)}}{2\sigma_1}\, \eta, \frac{\sigma_2}{2\sqrt{4\sigma_1\sigma_3 - \sigma_2^2}} \right), \tag{2.6}$$

$$F_2(\eta) = -\frac{\sigma_2}{4\sigma_1} \pm \frac{\sigma_2}{4\sigma_1}\, dn\left(\frac{\sigma_2}{4\sqrt{-\sigma_1}}\, \eta, \frac{2\sqrt{(4\sigma_1\sigma_3 - \sigma_2^2)}}{\sigma_2} \right). \tag{2.7}$$

Subcase 1.2. If $\sigma_1 < 0,\ (4\sigma_1\sigma_3 - \sigma_2^2) < 0,\ and\ (16\sigma_1\sigma_3 - 5\sigma_2^2) < 0$, then

$$F_3(\eta) = -\frac{\sigma_2}{4\sigma_1} \pm \frac{\sqrt{-(16\sigma_1\sigma_3 - 5\sigma_2^2)}}{4\sigma_1}\, cn\left(\frac{\sqrt{\sigma_1(4\sigma_1\sigma_3 - \sigma_2^2)}}{2\sigma_1}\, \eta, \frac{\sqrt{(4\sigma_1\sigma_3 - \sigma_2^2)(16\sigma_1\sigma_3 - 5\sigma_2^2)}}{2(4\sigma_1\sigma_3 - \sigma_2^2)} \right), \tag{2.8}$$

$$F_4(\eta) = -\frac{\sigma_2}{4\sigma_1} \pm \frac{\sqrt{-(16\sigma_1\sigma_3 - 5\sigma_2^2)}}{4\sigma_1}\, dn\left(\frac{\sqrt{\sigma_1(16\sigma_1\sigma_3 - 5\sigma_2^2)}}{4\sigma_1}\,\eta, \frac{2\sqrt{(4\sigma_1\sigma_3 - \sigma_2^2)(16\sigma_1\sigma_3 - 5\sigma_2^2)}}{16\sigma_1\sigma_3 - 5\sigma_2^2}\right). \tag{2.9}$$

Subcase 1.3. If $\sigma_1 < 0,\ (4\sigma_1\sigma_3 - \sigma_2^2) > 0$, and $(16\sigma_1\sigma_3 - 5\sigma_2^2) < 0$, then

$$F_5(\eta) = -\frac{\sigma_2}{4\sigma_1} \pm \frac{\sqrt{-(16\sigma_1\sigma_3 - 5\sigma_2^2)}}{4\sigma_1}\, nc\left(\frac{\sqrt{-\sigma_1(4\sigma_1\sigma_3 - \sigma_2^2)}}{2\sigma_1}\,\eta, \frac{\sigma_2}{2\sqrt{4\sigma_1\sigma_3 - \sigma_2^2}}\right), \tag{2.10}$$

$$F_6(\eta) = -\frac{\sigma_2}{4\sigma_1} \pm \frac{\sqrt{-(16\sigma_1\sigma_3 - 5\sigma_2^2)}}{4\sigma_1}\, nd\left(\frac{\sigma_2}{4\sqrt{-\sigma_1}}\,\eta, \frac{2\sqrt{(4\sigma_1\sigma_3 - \sigma_2^2)}}{\sigma_2}\right). \tag{2.11}$$

Subcase 1.4. If $(4\sigma_1\sigma_3 - \sigma_2^2) > 0,\ (4\sigma_1\sigma_3 - \sigma_2^2)(16\sigma_1\sigma_3 - 5\sigma_2^2) > 0$, then

$$F_7(\eta) = -\frac{\sigma_2}{4\sigma_1} \pm \frac{\sigma_2}{4\sigma_1}\, nc\left(\frac{\sqrt{\sigma_1(4\sigma_1\sigma_3 - \sigma_2^2)}}{2\sigma_1}\,\eta, \frac{\sqrt{(4\sigma_1\sigma_3 - \sigma_2^2)(16\sigma_1\sigma_3 - 5\sigma_2^2)}}{2(4\sigma_1\sigma_3 - \sigma_2^2)}\right), \tag{2.12}$$

$$F_8(\eta) = -\frac{\sigma_2}{4\sigma_1} \pm \frac{\sigma_2}{4\sigma_1}\, nd\left(\frac{\sqrt{\sigma_1(16\sigma_1\sigma_3 - 5\sigma_2^2)}}{4\sigma_1}\,\eta, \frac{2\sqrt{(4\sigma_1\sigma_3 - \sigma_2^2)(16\sigma_1\sigma_3 - 5\sigma_2^2)}}{16\sigma_1\sigma_3 - 5\sigma_2^2}\right). \tag{2.13}$$

Subcase 1.5. If $\sigma_1 > 0,\ (16\sigma_1\sigma_3 - 5\sigma_2^2) < 0$, then

$$F_9(\eta) = -\frac{\sigma_2}{4\sigma_1} \pm \frac{\sigma_2}{4\sigma_1}\, ns\left(\frac{\sigma_2}{4\sqrt{\sigma_1}}\eta, \frac{\sqrt{-(16\sigma_1\sigma_3 - 5\sigma_2^2)}}{\sigma_2}\right), \tag{2.14}$$

$$F_{10}(\eta) = -\frac{\sigma_2}{4\sigma_1} \pm \frac{\sqrt{-(16\sigma_1\sigma_3 - 5\sigma_2^2)}}{4\sigma_1}\, ns\left(\frac{\sqrt{-\sigma_1(16\sigma_1\sigma_3 - 5\sigma_2^2)}}{4\sigma_1}\,\eta, \frac{\sigma_2}{\sqrt{-(16\sigma_1\sigma_3 - 5\sigma_2^2)}}\right), \tag{2.15}$$

$$F_{11}(\eta) = -\frac{\sigma_2}{4\sigma_1} \pm \frac{\sqrt{-(16\sigma_1\sigma_3 - 5\sigma_2^2)}}{4\sigma_1}\, sn\left(\frac{\sigma_2}{4\sqrt{\sigma_1}}\,\eta, \frac{\sqrt{-(16\sigma_1\sigma_3 - 5\sigma_2^2)}}{\sigma_2}\right), \tag{2.16}$$

$$F_{12}(\eta) = -\frac{\sigma_2}{4\sigma_1} \pm \frac{\sigma_2}{4\sigma_1}\, sn\left(\frac{\sqrt{-\sigma_1(16\sigma_1\sigma_3 - 5\sigma_2^2)}}{4\sigma_1}\,\eta, \frac{\sigma_2}{\sqrt{-(16\sigma_1\sigma_3 - 5\sigma_2^2)}}\right). \tag{2.17}$$

The second argument of the Jacobi elliptic functions described above represents its elliptic modulus. For instance, in $sn(\eta, \Bbbk)$, $\Bbbk$ is the modulus of the elliptic function.

Case 2. When $\sigma_4 = \frac{\sigma_2(4\sigma_1\sigma_3-\sigma_2^2)}{8\sigma_1^2}$, $\sigma_5 = \frac{(4\sigma_1\sigma_3-\sigma_2^2)^2}{64\sigma_1^3}$. Consequently, Eq (2.5) have hyperbolic and trigonometric solutions.

Subcase 2.1. If $\sigma_1 > 0,\ (8\sigma_1\sigma_3 - 3\sigma_2^2) < 0$, then

$$F_{13}(\eta) = -\frac{\sigma_2}{4\sigma_1} \pm \frac{\sqrt{-(8\sigma_1\sigma_3 - 3\sigma_2^2)}}{4\sigma_1} \tanh\left(\frac{\sqrt{-\sigma_1(8\sigma_1\sigma_3 - 3\sigma_2^2)}}{4\sigma_1}\eta\right), \tag{2.18}$$

$$F_{14}(\eta) = -\frac{\sigma_2}{4\sigma_1} \pm \frac{\sqrt{-(8\sigma_1\sigma_3 - 3\sigma_2^2)}}{4\sigma_1} \coth\left(\frac{\sqrt{-\sigma_1(8\sigma_1\sigma_3 - 3\sigma_2^2)}}{4\sigma_1}\eta\right). \tag{2.19}$$

Subcase 2.2. If $\sigma_1 > 0,\ (8\sigma_1\sigma_3 - 3\sigma_2^2) > 0$, then

$$F_{15}(\eta) = -\frac{\sigma_2}{4\sigma_1} \pm \frac{\sqrt{(8\sigma_1\sigma_3 - 3\sigma_2^2)}}{4\sigma_1} \tan\left(\frac{\sqrt{\sigma_1(8\sigma_1\sigma_3 - 3\sigma_2^2)}}{4\sigma_1}\eta\right), \tag{2.20}$$

$$F_{16}(\eta) = -\frac{\sigma_2}{4\sigma_1} \pm \frac{\sqrt{(8\sigma_1\sigma_3 - 3\sigma_2^2)}}{4\sigma_1} \cot\left(\frac{\sqrt{\sigma_1(8\sigma_1\sigma_3 - 3\sigma_2^2)}}{4\sigma_1}\eta\right). \tag{2.21}$$

Case 3. When $\sigma_4 = \frac{\sigma_2(4\sigma_1\sigma_3-\sigma_2^2)}{8\sigma_1^2}$, $\sigma_5 = \frac{\sigma_2^2(16\sigma_1\sigma_3-5\sigma_2^2)}{256\sigma_1^3}$. Consequently, Eq (2.5) have hyperbolic and trigonometric solutions.

Subcase 3.1. If $\sigma_1 < 0,\ (8\sigma_1\sigma_3 - 3\sigma_2^2) < 0$, then

$$F_{17}(\eta) = -\frac{\sigma_2}{4\sigma_1} \pm \frac{\sqrt{-2(8\sigma_1\sigma_3 - 3\sigma_2^2)}}{4\sigma_1} sech\left(\frac{\sqrt{2\sigma_1(8\sigma_1\sigma_3 - 3\sigma_2^2)}}{4\sigma_1}\eta\right). \tag{2.22}$$

Subcase 3.2. If $\sigma_1 > 0,\ (8\sigma_1\sigma_3 - 3\sigma_2^2) > 0$, then

$$F_{18}(\eta) = -\frac{\sigma_2}{4\sigma_1} \pm \frac{\sqrt{2(8\sigma_1\sigma_3 - 3\sigma_2^2)}}{4\sigma_1} csch\left(\frac{\sqrt{2\sigma_1(8\sigma_1\sigma_3 - 3\sigma_2^2)}}{4\sigma_1}\eta\right). \tag{2.23}$$

Subcase 3.3. If $\sigma_1 > 0,\ (8\sigma_1\sigma_3 - 3\sigma_2^2) < 0$, then

$$F_{19}(\eta) = -\frac{\sigma_2}{4\sigma_1} \pm \frac{\sqrt{-2(8\sigma_1\sigma_3 - 3\sigma_2^2)}}{4\sigma_1} \sec\left(\frac{\sqrt{-2\sigma_1(8\sigma_1\sigma_3 - 3\sigma_2^2)}}{4\sigma_1}\eta\right), \tag{2.24}$$

$$F_{20}(\eta) = -\frac{\sigma_2}{4\sigma_1} \pm \frac{\sqrt{-2(8\sigma_1\sigma_3 - 3\sigma_2^2)}}{4\sigma_1} \csc\left(\frac{\sqrt{-2\sigma_1(8\sigma_1\sigma_3 - 3\sigma_2^2)}}{4\sigma_1}\eta\right). \tag{2.25}$$

Case 4. If we substitute $\sigma_2 = \sigma_4 = \sigma_5 = 0, \sigma_3 > 0$. Thus, we obtain the solution of Eq (2.5) in the following form:

$$F_{21}(\eta) = \frac{4\rho\sigma_3}{\left(4\rho^2 e^{\sqrt{\sigma_3}\eta} - \sigma_1\sigma_3 e^{-\sqrt{\sigma_3}\eta}\right)}. \tag{2.26}$$

By setting $\sigma_1 = -\frac{4\rho^2}{\sigma_3}$, the solution of Eq (2.26) becomes

$$F_{22}(\eta) = \frac{\sigma_3}{2\rho} sech(-\sqrt{\sigma_3}\eta). \tag{2.27}$$

By setting $\sigma_1 = \frac{4\rho^2}{\sigma_3}$, the solution of Eq (2.26) becomes

$$F_{23}(\eta) = \frac{\sigma_3}{2\rho} csch(-\sqrt{\sigma_3}\eta). \tag{2.28}$$

2.2. The extended hyperbolic function technique

In accordance with the extended hyperbolic function method [16], solutions can be represented as finite series in the following manner:

$$F(\eta) = \sum_{j=0}^{N} \vartheta_j E^j, \quad \vartheta_N \neq 0, \tag{2.29}$$

where the constant ϑ_N is included, and Eq (2.29) corresponds to the following nonlinear differential equation:

$$E'(\eta) = E\sqrt{\varpi_1 + \varpi_2 E^2}, \quad \varpi_1, \varpi_2 \in \Re. \tag{2.30}$$

The value of N can be computed using the balancing rule for ordinary differential equations. By setting the coefficients of the powers of E equal to zero and applying Eqs (2.3), (2.29), and (2.30), we derive a system of algebraic equations. Solving this system allows us to determine all the values of the associated coefficients. The general solutions to the ordinary differential equation (2.30) can subsequently be classified into several distinct types.

Family 1. When $\varpi_1 < 0$ and $\varpi_2 > 0$, we have

$$E_1(\eta) = \sqrt{\frac{-\varpi_1}{\varpi_2}} \sec\left(\sqrt{-\varpi_1}(\eta + \eta_0)\right).$$

Family 2. When $\varpi_1 > 0$ and $\varpi_2 < 0$, we have

$$E_2(\eta) = \sqrt{\frac{\varpi_1}{-\varpi_2}} \operatorname{sech}\left(\sqrt{\varpi_1}(\eta + \eta_0)\right).$$

Family 3. When $\varpi_1 < 0$ and $\varpi_2 < 0$, we have

$$E_3(\eta) = \sqrt{\frac{-\varpi_1}{\varpi_2}} \csc\left(\sqrt{-\varpi_1}(\eta + \eta_0)\right).$$

Family 4. When $\varpi_1 > 0$ and $\varpi_2 = 0$, we obtain

$$E_4(\eta) = e^{\sqrt{\varpi_1(\eta+\eta_0)}}.$$

Family 5. When $\varpi_1 < 0$ and $\varpi_2 = 0$, we obtain

$$E_5(\eta) = \cos\left(\sqrt{-\varpi_1}(\eta+\eta_0)\right) + i\sin\left(\sqrt{-\varpi_1}(\eta+\eta_0)\right).$$

Family 6. When $\varpi_1 = 0$ and $\varpi_2 > 0$, we obtain

$$E_6(\eta) = \frac{\pm 1}{\sqrt{\varpi_2}(\eta+\eta_0)}.$$

Family 7. When $\varpi_1 = 0$ and $\varpi_2 < 0$, we obtain

$$E_7(\eta) = \frac{\pm i}{\sqrt{-\varpi_2}(\eta+\eta_0)}.$$

Family 8. When $\varpi_1 > 0$ and $\varpi_2 > 0$, we obtain

$$E_8(\eta) = -\sqrt{\frac{\varpi_1}{\varpi_2}}\,\mathrm{csch}\left(\sqrt{\varpi_1}(\eta+\eta_0)\right),$$

where η_0 is constant.

3. Application of the methods

The Kairat-II equation can be addressed using the following transformations to derive soliton solutions for Eq (1.1):

$$\mu(\varkappa,\tau) = \varphi(\eta), \quad \eta = \omega(\varkappa - \lambda\tau), \tag{3.1}$$

where $\varphi(\eta)$ characterizes the pulse shape, ω represents the wave number, and λ denotes the wave velocity. By substituting Eq (3.1) into Eq (1.1), we obtain the following result:

$$\varphi'' - 3\omega((\varphi')^2)' + \omega^2\varphi'''' = 0. \tag{3.2}$$

Integrating Eq (3.2) with respect to η yields

$$\varphi' - 3\omega(\varphi')^2 + \omega^2\varphi''' + c_0 = 0, \tag{3.3}$$

where c_0 represents the real integration constant. Assume $\varphi'(\eta) = \phi(\eta)$, where $\phi(\eta)$ represents the real function.

$$\phi - 3\omega(\phi)^2 + \omega^2\phi'' + c_0 = 0. \tag{3.4}$$

3.1. The Kumar–Malik method

By applying the homogeneous balancing principle and utilizing Eq (3.4), we have $N = 2$, according to the equilibrium between ϕ^2 and ϕ''. Thus, the solution can be formulated as

$$\phi(\eta) = \Xi_0 + \Xi_1 F(\eta) + \Xi_2 F(\eta)^2, \tag{3.5}$$

together with

$$F'(\eta) = \sqrt{\sigma_1 F(\eta)^4 + \sigma_2 F(\eta)^3 + \sigma_3 F(\eta)^2 + \sigma_4 F(\eta) + \sigma_5}, \tag{3.6}$$

where Ξ_0, Ξ_1, and Ξ_2 are the constants yet to be determined. By substituting Eqs (3.5) and (3.6) into Eq (3.4) and setting the coefficients of all powers of $F_i(\eta), i = 0, 1, 2, 3, 4$ equal to zero, we derive the following system of algebraic equations:

$$\begin{aligned}
&F^0(\eta) : \Xi_0 - 3\omega\Xi_0^2 + \frac{1}{2}\omega^2\Xi_1\sigma_4 + 2\omega^2\Xi_2\sigma_5 + c_0 = 0,\\
&F^1(\eta) : \omega^2\Xi_1\sigma_3 + 3\omega^2\Xi_2\sigma_4 - 6\omega\Xi_0\Xi_1 + \Xi_1 = 0,\\
&F^2(\eta) : \Xi_2 - 6\omega\Xi_0\Xi_2 - 3\omega\Xi_1^2 + \frac{3}{2}\omega^2\Xi_1\sigma_2 + 4\omega^2\Xi_2\sigma_3 = 0,\\
&F^3(\eta) : 2\omega^2\Xi_1\sigma_1 + 5\omega^2\Xi_2\sigma_2 - 6\omega\Xi_1\Xi_2 = 0,\\
&F^4(\eta) : 6\omega^2\Xi_2\sigma_1 - 3\omega\Xi_2^2 = 0.
\end{aligned} \tag{3.7}$$

Case 1. With the parameters $\sigma_4 = \frac{\sigma_2\left(4\sigma_1\sigma_3 - \sigma_2^2\right)}{8\sigma_1^2}$, $\sigma_5 = 0$, the solution of system (3.5) is

$$\begin{aligned}
&\Xi_0 = \frac{16\omega^2\sigma_1\sigma_3 - 3\omega^2\sigma_2^2 + 4\sigma_1}{24\sigma_1\omega}, \quad \Xi_1 = \omega\sigma_2, \quad \Xi_2 = 2\omega\sigma_1,\\
&c_0 = \frac{256\omega^4\sigma_1^2\sigma_3^2 - 144\omega^4\sigma_1\sigma_2^2\sigma_3 + 21\omega^4\sigma_2^4 - 16\sigma_1^2}{192\omega\sigma_1^2}.
\end{aligned} \tag{3.8}$$

Substituting Eq (3.8) into Eq (3.5) yields the following general solution for Eq (1.1):

$$\phi(\eta) = \frac{16\omega^2\sigma_1\sigma_3 - 3\omega^2\sigma_2^2 + 4\sigma_1}{24\sigma_1\omega} + \omega\sigma_2 F(\eta) + 2\omega\sigma_1 F(\eta)^2. \tag{3.9}$$

For the solution of (3.9), we have $\varphi'(\eta) = \phi(\eta) \;\Rightarrow\; \varphi(\eta) = \int \phi(\eta) d\eta$,

$$\varphi(\eta) = \int \left(\frac{16\omega^2\sigma_1\sigma_3 - 3\omega^2\sigma_2^2 + 4\sigma_1}{24\sigma_1\omega} + \omega\sigma_2 F(\eta) + 2\omega\sigma_1 F(\eta)^2 \right) d\eta. \tag{3.10}$$

Subcase 1.1. If $\sigma_1 < 0$, $(4\sigma_1\sigma_3 - \sigma_2^2) > 0$. The traveling wave solution is given by

$$\mu_1(\varkappa, \tau) = -\frac{\eta\sigma_2\omega\left(2\sqrt{4\sigma_1\sigma_3 - \sigma_2^2} + \sigma_2\right)}{8\sigma_1} + \frac{4\eta\sigma_3\omega^2 + \eta}{6\omega} + \frac{\sigma_2\omega\mathcal{E}\left(\frac{\eta\sqrt{\sigma_1\left(\sigma_2^2 - 4\sigma_1\sigma_3\right)}}{2\sigma_1}, \frac{\sigma_2}{2\sqrt{4\sigma_1\sigma_3 - \sigma_2^2}}\right)}{2\sqrt{-\sigma_1}}, \tag{3.11}$$

$$\mu_2(\varkappa,\tau)=\eta\left(\frac{1}{6\omega}-\frac{\sigma_2^2\omega}{4\sigma_1}+\frac{2\sigma_3\omega}{3}\right)-\frac{\sigma_2\omega\mathcal{E}\left(\frac{\eta\sigma_2}{4\sqrt{-\sigma_1}},\frac{2\sqrt{-\sigma_2^2+4\sigma_1\sigma_3}}{\sigma_2}\right)}{2\sqrt{-\sigma_1}}. \tag{3.12}$$

Subcase 1.2. If $\sigma_1<0$, $(4\sigma_1\sigma_3-\sigma_2^2)<0$, and $(16\sigma_1\sigma_3-5\sigma_2^2)<0$. The traveling wave solution is given by

$$\begin{aligned}\mu_3(\varkappa,\tau)=&\frac{\eta}{8\sigma_1\sqrt{(\sigma_2^2-4\sigma_1\sigma_3)(5\sigma_2^2-16\sigma_1\sigma_3)\omega}}\\
&\times\left(10\sigma_2^4+3\sigma_2^2\left(\sqrt{(\sigma_2^2-4\sigma_1\sigma_3)(5\sigma_2^2-16\sigma_1\sigma_3)}-24\sigma_1\sigma_3\right)\right.\\
&+16\sigma_1\sigma_3\left(-\sqrt{(\sigma_2^2-4\sigma_1\sigma_3)(5\sigma_2^2-16\sigma_1\sigma_3)}+8\sigma_1\sigma_3\right)\omega^2\\
&\left.+4\sigma_1\sqrt{(\sigma_2^2-4\sigma_1\sigma_3)(5\sigma_2^2-16\sigma_1\sigma_3)}(1+4\sigma_3^2\omega)\right)\\
&-12\sigma_1(5\sigma_2^2-16\sigma_1\sigma_3)(\sigma_2^2-4\sigma_1\sigma_3)\omega^2\,\mathcal{E}\left(\frac{\eta\sqrt{\sigma_1(-\sigma_2^2+4\sigma_1\sigma_3)}}{2\sigma_1},-\frac{\sqrt{(\sigma_2^2-4\sigma_1\sigma_3)(5\sigma_2^2-16\sigma_1\sigma_3)}}{2\sigma_2^2-8\sigma_1\sigma_3}\right),\end{aligned} \tag{3.13}$$

$$\mu_4(\varkappa,\tau)=\eta\left(\frac{1}{6\omega}-\frac{\sigma_2^2\omega}{4\sigma_1}+\frac{2\sigma_3\omega}{3}\right)+\frac{\sqrt{5\sigma_2^2-16\sigma_1\sigma_3}\omega\,\mathcal{E}\left(\frac{\eta\sqrt{\sigma_1(-5\sigma_2^2+16\sigma_1\sigma_3)}}{2\sigma_1},-\frac{2(\sigma_2^2-4\sigma_1\sigma_3)}{\sqrt{(\sigma_2^2-4\sigma_1\sigma_3)(5\sigma_2^2-16\sigma_1\sigma_3)}}\right)}{4\sqrt{-\sigma_1}}. \tag{3.14}$$

Subcase 1.3. If $\sigma_1<0$, $(4\sigma_1\sigma_3-\sigma_2^2)>0$, and $(16\sigma_1\sigma_3-5\sigma_2^2)<0$. The traveling wave solution is given by

$$\begin{aligned}\mu_5(\varkappa,\tau)=&\frac{\eta\left(4+\frac{(9\sigma_2^2+16\sigma_1\sigma_3-48\sigma_1\sigma_3)\omega^2}{\sigma_1}\right)}{24\omega}\\
&+\frac{\sqrt{\sigma_1(\sigma_2^2-4\sigma_1\sigma_3)}(5\sigma_2^2-16\sigma_1\sigma_3)\omega}{2\sigma_1\left(8\sigma_1\sigma_3-\sigma_2(2\sigma_2+\sqrt{-\sigma_2^2+4\sigma_1\sigma_3})\mathrm{cn}\left(\frac{\eta\sqrt{\sigma_1(\sigma_2^2-4\sigma_1\sigma_3)}}{2\sigma_1},\frac{\sigma_2}{2\sqrt{-\sigma_2^2+4\sigma_1\sigma_3}}\right)\right)}\\
&\times\left(\mathrm{cn}\left(\frac{\eta\sqrt{\sigma_1(\sigma_2^2-4\sigma_1\sigma_3)}}{2\sigma_1},\frac{\sigma_2}{2\sqrt{-\sigma_2^2+4\sigma_1\sigma_3}}\right)\mathcal{E}\left(\frac{\eta\sqrt{\sigma_1(\sigma_2^2-4\sigma_1\sigma_3)}}{2\sigma_1},\frac{\sigma_2}{2\sqrt{-\sigma_2^2+4\sigma_1\sigma_3}}\right)\right.\\
&\left.-\mathrm{dn}\left(\frac{\eta\sqrt{\sigma_1(\sigma_2^2-4\sigma_1\sigma_3)}}{2\sigma_1},\frac{\sigma_2}{2\sqrt{-\sigma_2^2+4\sigma_1\sigma_3}}\right)\mathrm{sn}\left(\frac{\eta\sqrt{\sigma_1(\sigma_2^2-4\sigma_1\sigma_3)}}{2\sigma_1},\frac{\sigma_2}{2\sqrt{-\sigma_2^2+4\sigma_1\sigma_3}}\right)\right),\end{aligned} \tag{3.15}$$

$$\mu_6(\varkappa,\tau)=\frac{1}{12\sigma_1\left(\sigma_2-2\sqrt{\left(-\sigma_2^2+4\sigma_1\sigma_3\right)}\right)\omega}\left(\eta\left(-\sigma_2+2\sqrt{-\sigma_2^2+4\sigma_1\sigma_3)}\right)\left(3\sigma_2^2\omega^2-2\sigma_1\left(1+4\sigma_3\omega^2\right)\right)\right.$$
$$+6\sqrt{-\sigma_1}\left(5\sigma_2^2-16\sigma_1\sigma_3\right)\omega^2\mathcal{E}\left(\frac{\eta\sigma_2}{4\sqrt{-\sigma_1}},\frac{2\sqrt{-\sigma_2^2+4\sigma_1\sigma_3}}{\sigma_2}\right)$$
$$\left.+\frac{12\sqrt{-\sigma_1}\sqrt{-\sigma_2^2+4\sigma_1\sigma_3)}\left(-5\sigma_2^2+16\sigma_1\sigma_3\right)\omega^2\mathrm{cn}\left(\frac{\eta\sigma_2}{4\sqrt{-\sigma_1}},\frac{2\sqrt{-\sigma_2^2+4\sigma_1\sigma_3}}{\sigma_2}\right)\mathrm{sn}\left(\frac{\eta\sigma_2}{4\sqrt{-\sigma_1}},\frac{2\sqrt{-\sigma_2^2+4\sigma_1\sigma_3}}{\sigma_2}\right)}{\sigma_2\mathrm{dn}\left(\frac{\eta\sigma_2}{4\sqrt{-\sigma_1}},\frac{2\sqrt{-\sigma_2^2+4\sigma_1\sigma_3}}{\sigma_2}\right)}\right). \tag{3.16}$$

Subcase 1.4. If $(4\sigma_1\sigma_3-\sigma_2^2)>0,\ (4\sigma_1\sigma_3-\sigma_2^2)(16\sigma_1\sigma_3-5\sigma_2^2)>0$. The traveling wave solution is given by

$$\mu_7(\varkappa,\tau)=\eta\left(\frac{1}{6\omega}-\frac{\sigma_2^2\omega}{4\sigma_1}+\frac{2\sigma_3\omega}{3}\right)-\frac{1}{2\sqrt{\sigma_1\left(-\sigma_2^2+4\sigma_1\sigma_3\right)}}$$
$$\times\left(-2\sigma_2^2+8\sigma_1\sigma_3+\sqrt{\left(5\sigma_2^2-16\sigma_1\sigma_3\right)\left(\sigma_2^2-4\sigma_1\sigma_3\right)}\right)\omega$$
$$\times\left(\frac{\eta\left(2\sigma_2^2-8\sigma_1\sigma_3+\sqrt{\left(5\sigma_2^2-16\sigma_1\sigma_3\right)\left(\sigma_2^2-4\sigma_1\sigma_3\right)}\right)}{4\sqrt{\sigma_1\left(\left(-\sigma_2^2+4\sigma_1\sigma_3\right)\right)}}\right.$$
$$+\mathcal{E}\left(\frac{\eta\sqrt{\sigma_1\left(-\sigma_2^2+4\sigma_1\sigma_3\right)}}{2\sigma_1},-\frac{\sqrt{\left(5\sigma_2^2-16\sigma_1\sigma_3\right)\left(\sigma_2^2-4\sigma_1\sigma_3\right)}}{2\left(\sigma_2^2-4\sigma_1\sigma_3\right)}\right)$$
$$-\frac{1}{\mathrm{cn}\left(\frac{\eta\sqrt{\sigma_1\left(-\sigma_2^2+4\sigma_1\sigma_3\right)}}{2\sigma_1},-\frac{\sqrt{\left(5\sigma_2^2-16\sigma_1\sigma_3\right)\left(\sigma_2^2-4\sigma_1\sigma_3\right)}}{2\left(\sigma_2^2-4\sigma_1\sigma_3\right)}\right)}$$
$$\times\mathrm{dn}\left(\frac{\eta\sqrt{\sigma_1\left(-\sigma_2^2+4\sigma_1\sigma_3\right)}}{2\sigma_1},-\frac{\sqrt{\left(5\sigma_2^2-16\sigma_1\sigma_3\right)\left(\sigma_2^2-4\sigma_1\sigma_3\right)}}{2\left(\sigma_2^2-4\sigma_1\sigma_3\right)}\right)$$
$$\left.\times\mathrm{sn}\left(\frac{\eta\sigma_2}{4\sqrt{-\sigma_1}},\frac{2\sqrt{-\sigma_2^2+4\sigma_1\sigma_3}}{\sigma_2}\right)\right), \tag{3.17}$$

$$\mu_8(\varkappa,\tau)=\eta\left(\frac{1}{6\omega}-\frac{\sigma_2^2\omega}{4\sigma_1}+\frac{2\sigma_3\omega}{3}\right)+\frac{1}{\left(2\sqrt{\sigma_1\left(\left(-5\sigma_2^2+16\sigma_1\sigma_3\right)\right)}\left(-1+\frac{-2\sigma_2^2+8\sigma_1\sigma_3}{\sqrt{\left(5\sigma_2^2-16\sigma_1\sigma_3\right)\left(\sigma_2^2-4\sigma_1\sigma_3\right)}}\right)\right)}$$

$$\times\left(\sigma_2^2\omega\left(-\mathcal{E}\left(\frac{\eta\sqrt{\sigma_1\left(-5\sigma_2^2+16\sigma_1\sigma_3\right)}}{4\sigma_1},\frac{-2\left(\sigma_2^2-4\sigma_1\sigma_3\right)}{\sqrt{\left(5\sigma_2^2-16\sigma_1\sigma_3\right)\left(\sigma_2^2-4\sigma_1\sigma_3\right)}}\right)\right.\right.$$
$$-\frac{2\left(\sigma_2^2-4\sigma_1\sigma_3\right)}{\sqrt{\left(5\sigma_2^2-16\sigma_1\sigma_3\right)\left(\sigma_2^2-4\sigma_1\sigma_3\right)}\mathrm{dn}\left(\frac{\eta\sqrt{\sigma_1\left(-5\sigma_2^2+16\sigma_1\sigma_3\right)}}{4\sigma_1},\frac{-2\left(\sigma_2^2-4\sigma_1\sigma_3\right)}{\sqrt{\left(5\sigma_2^2-16\sigma_1\sigma_3\right)\left(\sigma_2^2-4\sigma_1\sigma_3\right)}}\right)}$$
$$\times\mathrm{cn}\left(\frac{\eta\sqrt{\sigma_1\left(-5\sigma_2^2+16\sigma_1\sigma_3\right)}}{4\sigma_1},\frac{-2\left(\sigma_2^2-4\sigma_1\sigma_3\right)}{\sqrt{\left(5\sigma_2^2-16\sigma_1\sigma_3\right)\left(\sigma_2^2-4\sigma_1\sigma_3\right)}}\right)$$
$$\left.\left.\times\mathrm{sn}\left(\frac{\eta\sqrt{\sigma_1\left(-5\sigma_2^2+16\sigma_1\sigma_3\right)}}{4\sigma_1},\frac{-2\left(\sigma_2^2-4\sigma_1\sigma_3\right)}{\sqrt{\left(5\sigma_2^2-16\sigma_1\sigma_3\right)\left(\sigma_2^2-4\sigma_1\sigma_3\right)}}\right)\right)\right). \tag{3.18}$$

Subcase 1.5. If $\sigma_1 > 0,\ (16\sigma_1\sigma_3 - 5\sigma_2^2) < 0$. The traveling wave solution is given by

$$\mu_9(\varkappa,\tau) = -\frac{\sigma_2\omega}{2\sqrt{\sigma_1}}\times\left(\mathrm{cs}\left(\frac{\eta\sigma_2}{4\sqrt{\sigma_1}},\frac{\sqrt{5\sigma_2^2-16\sigma_1\sigma_3}}{\sigma_2}\right)\mathrm{dn}\left(\frac{\eta\sigma_2}{4\sqrt{\sigma_1}},\frac{\sqrt{5\sigma_2^2-16\sigma_1\sigma_3}}{\sigma_2}\right)\right.$$
$$\left.+\eta\left(\frac{1}{6\omega}-\frac{\sigma_2^2\omega}{4\sigma_1}+\frac{2\sigma_3\omega}{3}\right)+\mathcal{E}\left(\frac{\eta\sigma_2}{4\sqrt{\sigma_1}},\frac{\sqrt{5\sigma_2^2-16\sigma_1\sigma_3}}{\sigma_2}\right)\right), \tag{3.19}$$

$$\mu_{10}(\varkappa,\tau) = \frac{1}{24\sigma_1\omega}\left(4\eta\sigma_1+\eta\left(9\sigma_2^2-32\sigma_1\sigma_3\right)\omega^2-12\omega^2\sqrt{\sigma_1\left(5\sigma_2^2-16\sigma_1\sigma_3\right)}\right.$$
$$\times\left(\mathrm{cs}\left(\frac{\eta\sqrt{\sigma_1\left(5\sigma_2^2-16\sigma_1\sigma_3\right)}}{4\sigma_1},\frac{\sigma_2}{\sqrt{5\sigma_2^2-16\sigma_1\sigma_3}}\right)\mathrm{dn}\left(\frac{\eta\sqrt{\sigma_1\left(5\sigma_2^2-16\sigma_1\sigma_3\right)}}{4\sigma_1},\frac{\sigma_2}{\sqrt{5\sigma_2^2-16\sigma_1\sigma_3}}\right)\right.$$
$$\left.\left.+\mathcal{E}\left(\frac{\eta\sqrt{\sigma_1\left(5\sigma_2^2-16\sigma_1\sigma_3\right)}}{4\sigma_1},\frac{\sigma_2}{\sqrt{5\sigma_2^2-16\sigma_1\sigma_3}}\right)\right)\right), \tag{3.20}$$

$$\mu_{11}(\varkappa,\tau) = \frac{\eta\sigma_2\left(-2\sigma_2+\sqrt{5\sigma_2^2-16\sigma_1\sigma_3}\right)\omega}{8\sigma_1}+\frac{\eta\left(1+4\sigma_3\omega^2\right)}{6\omega}$$
$$-\frac{\sqrt{5\sigma_2^2-16\sigma_1\sigma_3}\,\mathcal{E}\left(\frac{\eta\sigma_2}{4\sqrt{\sigma_1}},\frac{\sqrt{5\sigma_2^2-16\sigma_1\sigma_3}}{\sigma_2}\right)}{2\sqrt{\sigma_1}}, \tag{3.21}$$

$$\mu_{12}(\varkappa,\tau)=\frac{\eta\sigma_2\left(-2\sigma_2+\sqrt{5\sigma_2^2-16\sigma_1\sigma_3}\right)\omega}{8\sigma_1}+\frac{\eta\left(1+4\sigma_3\omega^2\right)}{6\omega}-\frac{\sigma_2\omega\mathcal{E}\left(\frac{\eta\sqrt{\sigma_1\left(5\sigma_2^2-16\sigma_1\sigma_3\right)}}{4\sigma_1},\frac{\sigma_2}{\sqrt{5\sigma_2^2-16\sigma_1\sigma_3}}\right)}{2\sqrt{\sigma_1}}. \tag{3.22}$$

Case 2. When $\sigma_4=\frac{\sigma_2(4\sigma_1\sigma_3-\sigma_2^2)}{8\sigma_1^2}$, $\sigma_5=\frac{(4\sigma_1\sigma_3-\sigma_2^2)^2}{64\sigma_1^3}$, and the Eq (2.5) has hyperbolic and trigonometric solutions

$$\begin{aligned}&\Xi_0=\frac{16\omega^2\sigma_1\sigma_3-3\omega^2\sigma_2^2+4\sigma_1}{24\omega\sigma_1},\quad \Xi_1=\omega\sigma_2,\quad \Xi_2=2\omega\sigma_1,\\&c_0=\frac{64\omega^4\sigma_1^2\sigma_3^2-48\omega^4\sigma_1\sigma_2^2\sigma_3+9\omega^4\sigma_2^4-16\sigma_1^2}{192\sigma_1^2\omega}.\end{aligned} \tag{3.23}$$

Substituting Eq (3.23) into Eq (3.5) yields the following general solution for Eq (1.1):

$$\phi(\eta)=\frac{16\omega^2\sigma_1\sigma_3-3\omega^2\sigma_2^2+4\sigma_1}{24\sigma_1\omega}+\omega\sigma_2F(\eta)+2\omega\sigma_1F(\eta)^2. \tag{3.24}$$

For the solution of (3.24), we have $\varphi'(\eta)=\phi(\eta)\ \Rightarrow\ \varphi(\eta)=\int\phi(\eta)d\eta$

$$\varphi(\eta)=\int\left(\frac{16\omega^2\sigma_1\sigma_3-3\omega^2\sigma_2^2+4\sigma_1}{24\sigma_1\omega}+\omega\sigma_2F(\eta)+2\omega\sigma_1F(\eta)^2\right)d\eta. \tag{3.25}$$

Subcase 2.1. If $\sigma_1>0,\ (8\sigma_1\sigma_3-3\sigma_2^2)<0$. The traveling wave solution is given by

$$\mu_{13}(\varkappa,\tau)=\eta\left(\frac{1}{6\omega}-\frac{\sigma_2^2\omega}{4\sigma_1}+\frac{2\sigma_3\omega}{3}\right)-\frac{\sqrt{3\sigma_2^2-8\sigma_1\sigma_3}\omega}{2\sqrt{\sigma_1}}\tanh\left(\frac{\eta\sqrt{3\sigma_2^2-8\sigma_1\sigma_3}}{4\sqrt{\sigma_1}}\right), \tag{3.26}$$

$$\mu_{14}(\varkappa,\tau)=\eta\left(\frac{1}{6\omega}+\frac{\sigma_2^2\omega}{8\sigma_1}-\frac{\sigma_3\omega}{3}\right)-\frac{\sqrt{3\sigma_2^2-8\sigma_1\sigma_3}\omega}{2\sqrt{\sigma_1}}\coth\left(\frac{\eta\sqrt{3\sigma_2^2-8\sigma_1\sigma_3}}{4\sqrt{\sigma_1}}\right). \tag{3.27}$$

Subcase 2.2. If $\sigma_1>0,\ (8\sigma_1\sigma_3-3\sigma_2^2)>0$. The traveling wave solution is given by

$$\mu_{15}(\varkappa,\tau)=\eta\left(\frac{1}{6\omega}+\frac{\sigma_2^2\omega}{8\sigma_1}-\frac{\sigma_3\omega}{3}\right)+\frac{\sqrt{-3\sigma_2^2+8\sigma_1\sigma_3}\omega}{2\sqrt{\sigma_1}}\tan\left(\frac{\eta\sqrt{-3\sigma_2^2+8\sigma_1\sigma_3}}{4\sqrt{\sigma_1}}\right), \tag{3.28}$$

$$\mu_{16}(\varkappa,\tau)=\eta\left(\frac{1}{6\omega}+\frac{\sigma_2^2\omega}{8\sigma_1}-\frac{\sigma_3\omega}{3}\right)-\frac{\sqrt{-3\sigma_2^2+8\sigma_1\sigma_3}\omega}{2\sqrt{\sigma_1}}\cot\left(\frac{\eta\sqrt{-3\sigma_2^2+8\sigma_1\sigma_3}}{4\sqrt{\sigma_1}}\right). \tag{3.29}$$

Case 3. When $\sigma_4 = \frac{\sigma_2(4\sigma_1\sigma_3-\sigma_2^2)}{8\sigma_1^2}$, $\sigma_5 = \frac{\sigma_2^2(16\sigma_1\sigma_3-5\sigma_2^2)}{256\sigma_1^3}$, and the Eq (2.5) has hyperbolic and trigonometric solutions:

$$\begin{aligned}\Xi_0 &= \frac{16\omega^2\sigma_1\sigma_3 - 3\omega^2\sigma_2^2 + 4\sigma_1}{24\omega\sigma_1}, \quad \Xi_1 = \omega\sigma_2, \quad \Xi_2 = 2\omega\sigma_1,\\ c_0 &= \frac{64\omega^4\sigma_1^2\sigma_3^2 - 48\omega^4\sigma_1\sigma_2^2\sigma_3 + 9\omega^4\sigma_2^4 - 4\sigma_1^2}{48\sigma_1^2\omega}.\end{aligned} \tag{3.30}$$

Substituting Eq (3.30) into Eq (3.5) yields the following general solution for Eq (1.1):

$$\phi(\eta) = \frac{16\omega^2\sigma_1\sigma_3 - 3\omega^2\sigma_2^2 + 4\sigma_1}{24\sigma_1\omega} + \omega\sigma_2 F(\eta) + 2\omega\sigma_1 F(\eta)^2. \tag{3.31}$$

For the solution of (3.31), we have $\varphi'(\eta) = \phi(\eta) \Rightarrow \varphi(\eta) = \int \phi(\eta)d\eta$

$$\varphi(\eta) = \int \left(\frac{16\omega^2\sigma_1\sigma_3 - 3\omega^2\sigma_2^2 + 4\sigma_1}{24\sigma_1\omega} + \omega\sigma_2 F(\eta) + 2\omega\sigma_1 F(\eta)^2 \right) d\eta. \tag{3.32}$$

Subcase 3.1. If $\sigma_1 < 0,\ (8\sigma_1\sigma_3 - 3\sigma_2^2) < 0$. The traveling wave solution is given by

$$\mu_{17}(\varkappa,\tau) = \eta\left(\frac{1}{6\omega} - \frac{\sigma_2^2\omega}{4\sigma_1} + \frac{2\sigma_3\omega}{3}\right) - \frac{\sqrt{-3\sigma_2^2 + 8\sigma_1\sigma_3}\omega}{\sqrt{2\sigma_1}} \tanh\left(\frac{\eta\sqrt{-3\sigma_2^2 + 8\sigma_1\sigma_3}}{2\sqrt{2\sigma_1}}\right). \tag{3.33}$$

Subcase 3.2. If $\sigma_1 > 0,\ (8\sigma_1\sigma_3 - 3\sigma_2^2) > 0$. The traveling wave solution is given by

$$\mu_{18}(\varkappa,\tau) = \eta\left(\frac{1}{6\omega} - \frac{\sigma_2^2\omega}{4\sigma_1} + \frac{2\sigma_3\omega}{3}\right) - \frac{\sqrt{-3\sigma_2^2 + 8\sigma_1\sigma_3}\omega}{\sqrt{2\sigma_1}} \coth\left(\frac{\eta\sqrt{-3\sigma_2^2 + 8\sigma_1\sigma_3}}{2\sqrt{2\sigma_1}}\right). \tag{3.34}$$

Subcase 3.3. If $\sigma_1 > 0,\ (8\sigma_1\sigma_3 - 3\sigma_2^2) < 0$. The traveling wave solution is given by

$$\mu_{19}(\varkappa,\tau) = \eta\left(\frac{1}{6\omega} - \frac{\sigma_2^2\omega}{4\sigma_1} + \frac{2\sigma_3\omega}{3}\right) + \frac{\sqrt{3\sigma_2^2 - 8\sigma_1\sigma_3}\omega}{\sqrt{2\sigma_1}} \tan\left(\frac{\eta\sqrt{3\sigma_2^2 - 8\sigma_1\sigma_3}}{2\sqrt{2\sigma_1}}\right), \tag{3.35}$$

$$\mu_{20}(\varkappa,\tau) = \eta\left(\frac{1}{6\omega} - \frac{\sigma_2^2\omega}{4\sigma_1} + \frac{2\sigma_3\omega}{3}\right) - \frac{\sqrt{3\sigma_2^2 - 8\sigma_1\sigma_3}\omega}{\sqrt{2\sigma_1}} \cot\left(\frac{\eta\sqrt{3\sigma_2^2 - 8\sigma_1\sigma_3}}{2\sqrt{2\sigma_1}}\right). \tag{3.36}$$

Case 4. By substituting $\sigma_2 = \sigma_4 = \sigma_5 = 0, \sigma_3 > 0$. We then obtain the solution of Eq (2.5) in the following form:

$$\Xi_0 = \frac{4\omega^2\sigma_3 + 1}{6\omega}, \quad \Xi_1 = 0, \quad \Xi_2 = 2\omega\sigma_1, \quad c_0 = \frac{16\omega^4\sigma_3^2 - 1}{12\omega}. \tag{3.37}$$

Substituting Eq (3.37) into Eq (3.5) yields the following general solution for Eq (1.1):

$$\phi(\eta) = \frac{4\omega^2\sigma_3 + 1}{6\omega} + 2\omega\sigma_1 F(\eta)^2. \tag{3.38}$$

For the solution of (3.38), we have $\varphi'(\eta) = \phi(\eta) \;\Rightarrow\; \varphi(\eta) = \int \phi(\eta)d\eta$ with

$$\varphi(\eta) = \int \left(\frac{4\omega^2\sigma_3 + 1}{6\omega} + 2\omega\sigma_1 F(\eta)^2 \right) d\eta, \tag{3.39}$$

$$\mu_{21}(\varkappa, \tau) = \frac{4\sigma_1\sigma_3^{\frac{3}{2}}\omega}{-4e^{2\sqrt{\sigma_3}\eta}\rho^2 + \sigma_1\sigma_3} + \eta\left(\frac{1}{6\omega} - \frac{\sigma_2^2\omega}{8\sigma_1} + \frac{2\sigma_3\omega}{3} \right) - \frac{2\sigma_2\omega \tanh^{-1}\left(\frac{e^{2\sqrt{\sigma_3}\eta}\rho}{\sqrt{\sigma_1\sigma_3}} \right)}{\sqrt{\sigma_1}}, \tag{3.40}$$

$$\mu_{22}(\varkappa, \tau) = \eta\left(\frac{1}{6\omega} - \frac{\sigma_2^2\omega}{8\sigma_1} + \frac{2\sigma_3\omega}{3} \right) + \frac{\sigma_2\sqrt{\sigma_3}\omega \tanh^{-1}\left(\sinh\left(\eta\sqrt{\sigma_3} \right) \right)}{2\rho} + \frac{\sigma_1\sigma_3^{\frac{3}{2}}\omega \tanh\left(\eta\sqrt{\sigma_3} \right)}{2\rho^2}, \tag{3.41}$$

$$\begin{aligned} \mu_{23}(\varkappa, \tau) = {} & \eta\left(\frac{1}{6\omega} - \frac{\sigma_2^2\omega}{8\sigma_1} + \frac{2\sigma_3\omega}{3} \right) - \frac{\sqrt{\sigma_3}\omega}{2\rho^2}\left(\sigma_1\sigma_3 \coth\left(\eta\sqrt{\sigma_3} \right) \right) + \rho\sigma_2\left(-\log\left(\cosh\left(\frac{\eta\sqrt{\sigma_3}}{2} \right) \right) \right) \\ & + \log\left(\sinh\left(\frac{\eta\sqrt{\sigma_3}}{2} \right) \right). \end{aligned} \tag{3.42}$$

3.2. The extended hyperbolic function technique

In accordance with the homogeneous balancing principle, by applying Eq (3.4) and considering the Equation $N + 2 = 2N$, we determine that $N = 2$ on the basis of the equilibrium between ϕ^2 and ϕ''. Thus, the solution can be formulated as

$$\phi(\eta) = \vartheta_0 + \vartheta_1 E(\eta) + \vartheta_2 E(\eta)^2. \tag{3.43}$$

To find the derivative of Eq (3.43), we substitute it into Eq (3.4) along with Eq (2.30) and compare the coefficients of $E(\eta)$; this process results in a system of equations. Solving this system yields the following solution:

$$\begin{aligned} & E^0(\eta) : -3\omega\vartheta_0^2 + c_0 + \vartheta_0 = 0, \\ & E^1(\eta) : \omega^2\varpi_1\vartheta_1 - 6\omega\vartheta_0\vartheta_1 + \vartheta_1 = 0, \\ & E^2(\eta) : 4\omega^2\varpi_1\vartheta_2 - 6\omega\vartheta_0\vartheta_2 - 3\omega\vartheta_1^2 + \vartheta_2 = 0, \\ & E^3(\eta) : 2\omega^2\varpi_2\vartheta_1 - 6\omega\vartheta_1\vartheta_2 = 0, \\ & E^4(\eta) : 6\omega^2\varpi_2\vartheta_2 - 3\omega\vartheta_2^2 = 0. \end{aligned} \tag{3.44}$$

Using the Maple program, we applied it to uncover a solution for the given system, leading to a practical result.

Solution set.

$$\vartheta_0 = \frac{4\omega^2\varpi_1 + 1}{6\omega}, \quad \vartheta_1 = 0, \quad \vartheta_2 = 2\omega\varpi_2, \quad c_0 = \frac{16\omega^4\varpi_1^2 - 1}{12\omega}. \tag{3.45}$$

By substituting Eq (3.45) into Eq (3.43), we obtain the following general solution for Eq (1.1):

$$\phi(\eta) = \frac{4\omega^2\varpi_1 + 1}{6\omega} + 2\omega\varpi_2 E(\eta)^2. \tag{3.46}$$

For the solution of (3.46), we have $\varphi'(\eta) = \phi(\eta) \;\Rightarrow\; \varphi(\eta) = \int \phi(\eta)d\eta$ with

$$\varphi(\eta) = \int \left(\frac{4\omega^2\varpi_1 + 1}{6\omega} + 2\omega\varpi_2 E(\eta)^2 \right) d\eta. \tag{3.47}$$

Family 1. When $\varpi_1 < 0$ and $\varpi_2 > 0$, the traveling wave solution is given by

$$\mu_{F1}(\varkappa, \tau) = \frac{\eta}{6\omega} + \frac{2\eta\varpi_1\omega}{3} - 2\sqrt{\varpi_1}\omega \tanh\left(\eta\sqrt{\varpi_1} + \eta_0\sqrt{\varpi_1}\right). \tag{3.48}$$

Family 2. When $\varpi_1 > 0$ and $\varpi_2 < 0$, the traveling wave solution is given by

$$\mu_{F2}(\varkappa, \tau) = \frac{\eta}{6\omega} + \frac{2\eta\varpi_1\omega}{3} - 2\sqrt{\varpi_1}\omega \tanh\left(\eta\sqrt{\varpi_1} + \eta_0\sqrt{\varpi_1}\right). \tag{3.49}$$

Family 3. When $\varpi_1 < 0$ and $\varpi_2 < 0$, the traveling wave solution is given by

$$\mu_{F3}(\varkappa, \tau) = \frac{\eta}{6\omega} + \frac{2\eta\varpi_1\omega}{3} - 2\sqrt{\varpi_1}\omega \coth\left((\eta + \eta_0)\sqrt{\varpi_1}\right). \tag{3.50}$$

Family 4. When $\varpi_1 > 0$ and $\varpi_2 = 0$, the traveling wave solution is given by

$$\mu_{F4}(\varkappa, \tau) = \frac{\eta}{6\omega} + \frac{2\eta\varpi_1\omega}{3} + \frac{4e^{2\sqrt{\varpi_1(\eta+\eta_0)}\left(-\frac{3\varpi_2}{4} + \frac{3}{2}\sqrt{\varpi_1(\eta+\eta_0)}\varpi_2\right)\omega}}{3\varpi_1}. \tag{3.51}$$

Family 5. When $\varpi_1 < 0$ and $\varpi_2 = 0$, the traveling wave solution is given by

$$\mu_{F5}(\varkappa, \tau) = \frac{\eta}{6\omega} + \frac{2\eta\varpi_1\omega}{3} - \frac{ie^{2i\sqrt{-\varpi_1}(\eta+\eta_0)}\varpi_2\omega}{\sqrt{-\varpi_1}}. \tag{3.52}$$

Family 6. When $\varpi_1 < 0$ and $\varpi_2 = 0$, the traveling wave solution is given by

$$\mu_{F6}(\varkappa, \tau) = \frac{\eta}{6\omega} - \frac{2\omega}{\eta + \eta_0} + \frac{2(\eta + \eta_0)\varpi_1\omega}{3}. \tag{3.53}$$

Family 7. When $\varpi_1 < 0$ and $\varpi_2 = 0$, the traveling wave solution is given by

$$\mu_{F7}(\varkappa, \tau) = \frac{\eta}{6\omega} - \frac{2\omega}{\eta + \eta_0} + \frac{2(\eta + \eta_0)\varpi_1\omega}{3}. \tag{3.54}$$

Family 8. When $\varpi_1 < 0$ and $\varpi_2 = 0$, the traveling wave solution is given by

$$\mu_{F8}(\varkappa, \tau) = \frac{\eta}{6\omega} + \frac{2\eta\varpi_1\omega}{3} - 2\sqrt{\varpi_1}\omega \coth\left((\eta + \eta_0)\sqrt{\varpi_1}\right). \tag{3.55}$$

4. Results and discussion

The objective of this study was to employ Mathematica 13.3.1 as a computational framework to analyze the graphical properties of the nonlinear Kairat-II equation. The temporal evolution of wave propagation at varying velocities is illustrated through a suite of visualizations, including 2D, 3D, and contour diagrams. The investigation is conducted over the spatial and temporal domains $-20 \leq x \leq 20$ and $0 \leq t \leq 10$, respectively and encompasses a broad spectrum of parameter values for the relevant variables. The primary aims were to thoroughly examine the graphical behavior of the model and to elucidate the dynamic features that emerge from variations in the model's parameters. In solving the equation, a combination of trigonometric, exponential, and hyperbolic functions was utilized to comprehensively characterize the solution space.

This section delineates the behaviors and analytical interpretations of several obtained solutions, emphasizing the role of λ. The analysis is carried out graphically through the handling of Figures 1–9, which show the response of the soliton solution. As a sequel to the analysis, the following findings are established. Both sets of figures provide a view on how changes in the parameter λ influence the soliton. Subfigures (a), (d), and (g) consist of 3D plots that show the behaviour of the soliton solution with different values of λ. These plots enable one to track the soliton's dynamics, particularly its amplitude, width, and velocity. This aspect is particularly critical when analyzing soliton dynamics modeled by linear coupled stochastic differential equations (LCSDEs). It should be noted that subfigures (c), (f), and (i) address the 2D behavior of the soliton solution. These plots offer a clearer picture of the soliton's shape and how the propagation properties vary with λ. Subfigures (b), (e), and (h) are 2D contour plots that provide a top view of the soliton solution. These contour plots help determine the intensity distribution and the soliton's outline along the z-direction. These subfigures demonstrate the whole structure and stability of the soliton through a 3D top view. Altogether, these graphical illustrations provide a quantitative and visual perception of how the soliton behaves under different conditions, helping to extend the understanding of phenomena like stability measures, solitary wave encounters, and the time evolution within Solomon's mathematical model. Such plots are necessary for studying the soliton's behavior depending on the stability parameters and tracking the fine details of its dynamics.

The soliton solutions derived for the nonlinear Kairat-II equation provide valuable physical insights into optical pulse propagation in nonlinear media. These solutions illustrate how solitons maintain their stability while traveling through optical fibers, effectively balancing dispersion and nonlinearity to minimize signal distortion in high-speed communication systems. The Jacobi elliptic solutions describe periodic wave structures that transition into solitons under specific conditions, making them relevant to optical lattices and photonic crystals. The bright and dark solitons highlight distinct regimes of energy localization, which are crucial for designing optical switches, modulators, and pulse-shaping techniques. Additionally, the rational and singular solutions offer insights into localized energy concentration and wave collapse phenomena. The graphical analysis, including 2D, 3D, and contour plots, further demonstrates the solitons' stability and interactions under various parametric conditions. The diversity of soliton solutions provides a valuable framework for future research, as it simplifies the complexity of systems across various scientific domains, including fluid dynamics, optical fibers, and condensed matter physics. This reduction in complexity facilitates both practical applications and theoretical advancements, enabling deeper insights and innovative developments in these fields.

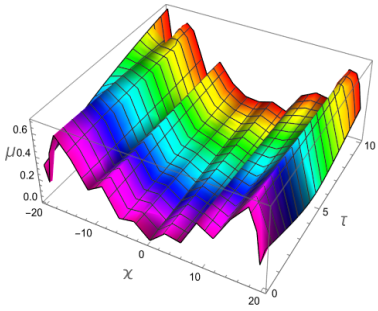

(a) Three-dimensional plot at $\sigma_1 = 0.01$, $\sigma_2 = 0.5$, $\sigma_3 = 1.2$, $\omega = 0.19$, and $\lambda = 0.1$.

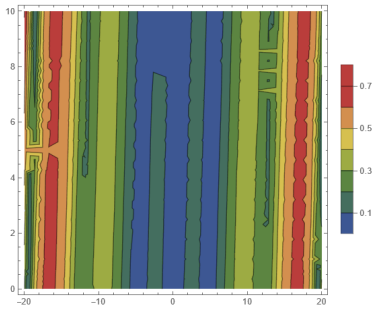

(b) Contour plot at $\sigma_1 = 0.01$, $\sigma_2 = 0.5$, $\sigma_3 = 1.2$, $\omega = 0.19$, and $\lambda = 0.1$.

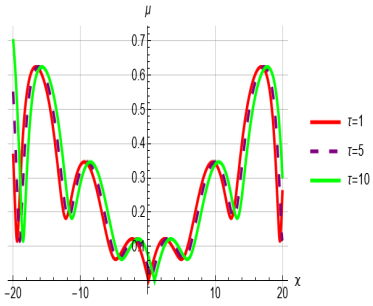

(c) Influence of time on the propagation of waves at $\sigma_1 = 0.01$, $\sigma_2 = 0.5$, $\sigma_3 = 1.2$, $\omega = 0.19$, and $\lambda = 0.1$.

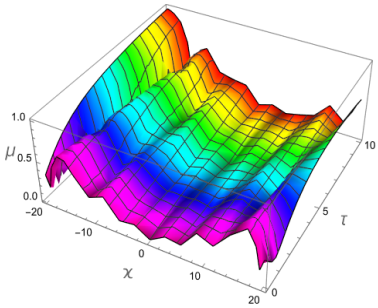

(d) Three-dimensional plot at $\sigma_1 = 0.01$, $\sigma_2 = 0.5$, $\sigma_3 = 1.2$, $\omega = 0.19$, and $\lambda = 0.5$.

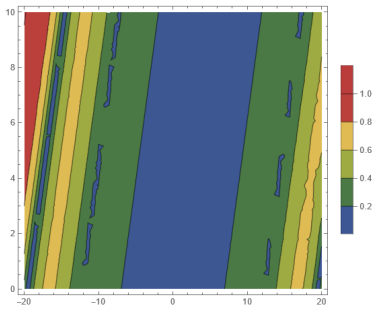

(e) Contour plot at $\sigma_1 = 0.01$, $\sigma_2 = 0.5$, $\sigma_3 = 1.2$, $\omega = 0.19$, and $\lambda = 0.5$.

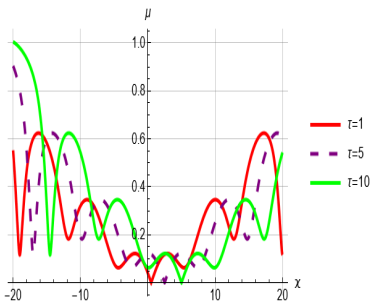

(f) Influence of time on the propagation of waves at $\sigma_1 = 0.01$, $\sigma_2 = 0.5$, $\sigma_3 = 1.2$, $\omega = 0.19$, and $\lambda = 0.5$.

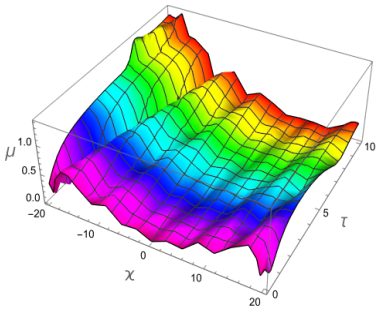

(g) Three-dimensional plot at $\sigma_1 = 0.01$, $\sigma_2 = 0.5$, $\sigma_3 = 1.2$, $\omega = 0.19$, and $\lambda = 1$.

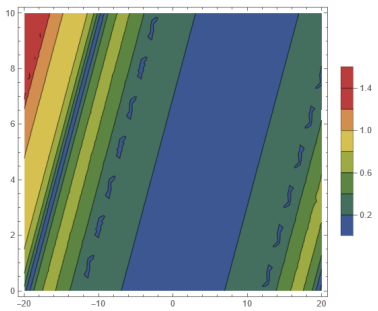

(h) Contour plot at $\sigma_1 = 0.01$, $\sigma_2 = 0.5$, $\sigma_3 = 1.2$, $\omega = 0.19$, and $\lambda = 1$.

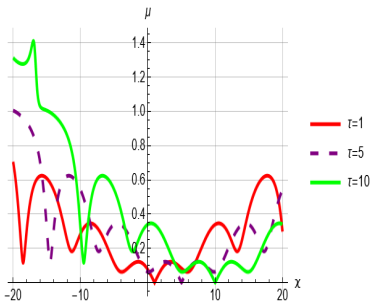

(i) Influence of time on the propagation of waves at $\sigma_1 = 0.01$, $\sigma_2 = 0.5$, $\sigma_3 = 1.2$, $\omega = 0.19$, and $\lambda = 1$.

Figure 1. Dynamic propagation of the soliton solution $\mu_1(\varkappa, \tau)$.

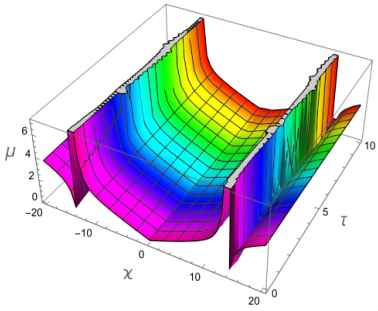

(a) Three-dimensional plot at $\sigma_1 = 0.01$, $\sigma_2 = 0.09$, $\sigma_3 = 1.5$, $\omega = 0.15$, and $\lambda = 0.1$.

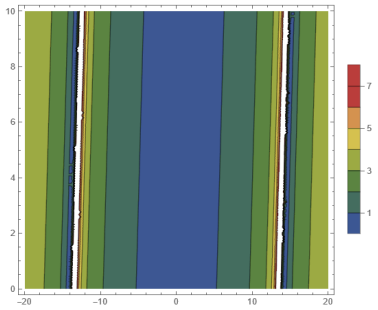

(b) Contour plot at $\sigma_1 = 0.01$, $\sigma_2 = 0.09$, $\sigma_3 = 1.5$, $\omega = 0.15$, and $\lambda = 0.1$.

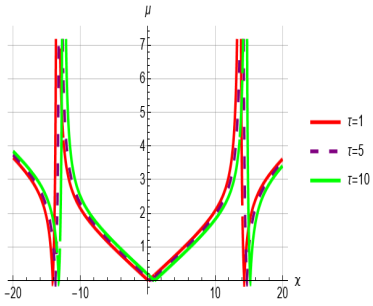

(c) Influence of time on the propagation of waves at $\sigma_1 = 0.01$, $\sigma_2 = 0.09$, $\sigma_3 = 1.5$, $\omega = 0.15$, and $\lambda = 0.1$.

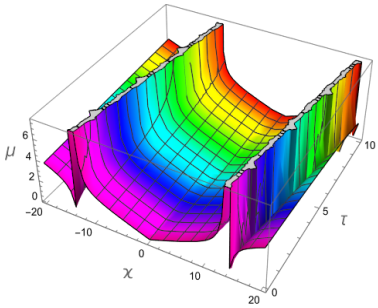

(d) Three-dimensional plot at $\sigma_1 = 0.01$, $\sigma_2 = 0.09$, $\sigma_3 = 1.5$, $\omega = 0.15$, and $\lambda = 0.5$.

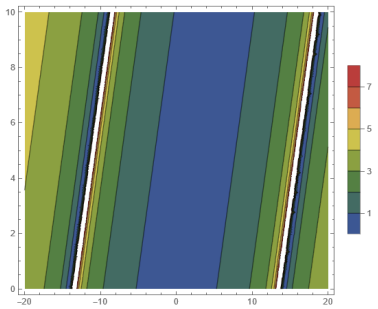

(e) Contour plot at $\sigma_1 = 0.01$, $\sigma_2 = 0.09$, $\sigma_3 = 1.5$, $\omega = 0.15$, and $\lambda = 0.5$.

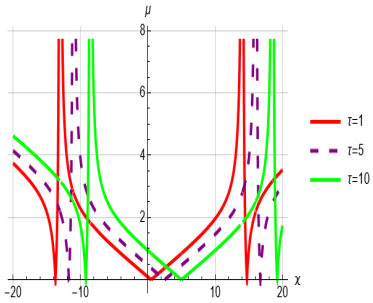

(f) Influence of time on the propagation of waves at $\sigma_1 = 0.01$, $\sigma_2 = 0.09$, $\sigma_3 = 1.5$, $\omega = 0.15$, and $\lambda = 0.5$.

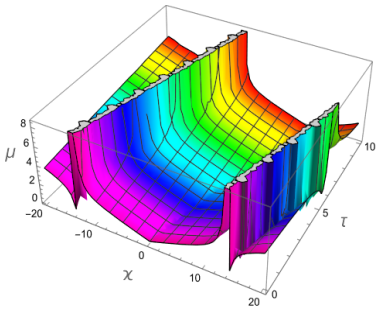

(g) Three-dimensional plot at $\sigma_1 = 0.01$, $\sigma_2 = 0.09$, $\sigma_3 = 1.5$, $\omega = 0.15$, and $\lambda = 1$.

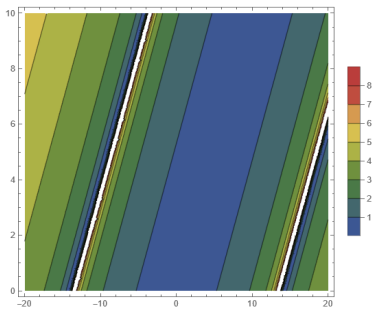

(h) Contour plot at $\sigma_1 = 0.01$, $\sigma_2 = 0.09$, $\sigma_3 = 1.5$, $\omega = 0.15$, and $\lambda = 1$.

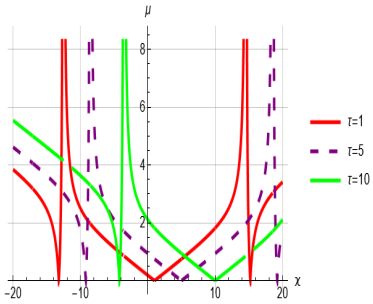

(i) Influence of time on the propagation of waves at $\sigma_1 = 0.01$, $\sigma_2 = 0.09$, $\sigma_3 = 1.5$, $\omega = 0.15$, and $\lambda = 1$.

Figure 2. Dynamic propagation of the soliton solution $\mu_{13}(\varkappa, \tau)$.

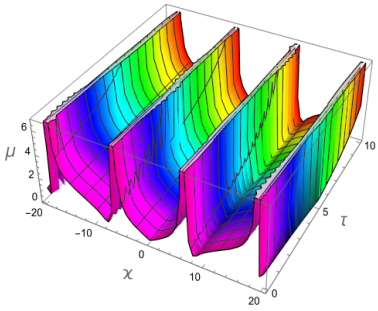

(a) Three-dimensional plot at $\sigma_1 = 0.125$, $\sigma_2 = 0.08$, $\sigma_3 = 0.08$, $\omega = 1.45$, and $\lambda = 0.1$.

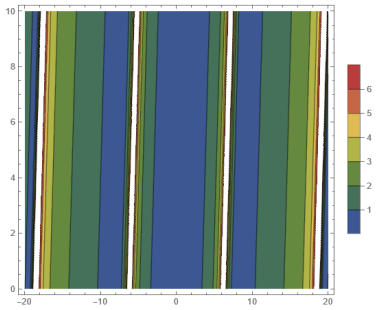

(b) Contour plot at $\sigma_1 = 0.125$, $\sigma_2 = 0.08$, $\sigma_3 = 0.08$, $\omega = 1.45$, and $\lambda = 0.1$.

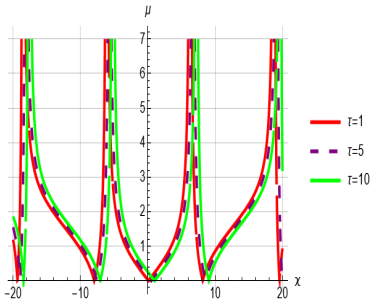

(c) Influence of time on the propagation of waves at $\sigma_1 = 0.125$, $\sigma_2 = 0.08$, $\sigma_3 = 0.08$, $\omega = 1.45$, and $\lambda = 0.1$.

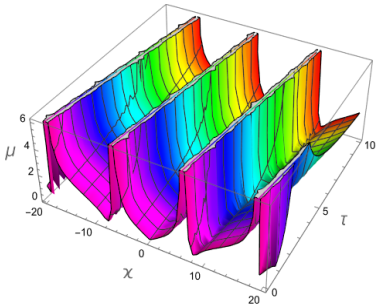

(d) Three-dimensional plot at $\sigma_1 = 0.125$, $\sigma_2 = 0.08$, $\sigma_3 = 0.08$, $\omega = 1.45$, and $\lambda = 0.5$.

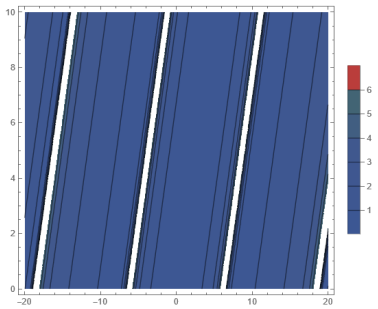

(e) Contour plot at $\sigma_1 = 0.125$, $\sigma_2 = 0.08$, $\sigma_3 = 0.08$, $\omega = 1.45$, and $\lambda = 0.5$.

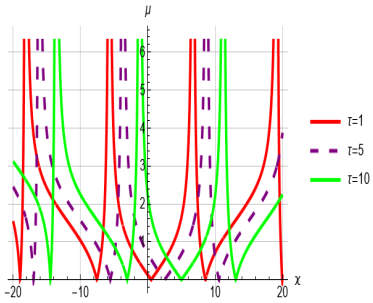

(f) Influence of time on the propagation of waves at $\sigma_1 = 0.125$, $\sigma_2 = 0.08$, $\sigma_3 = 0.08$, $\omega = 1.45$, and $\lambda = 0.5$.

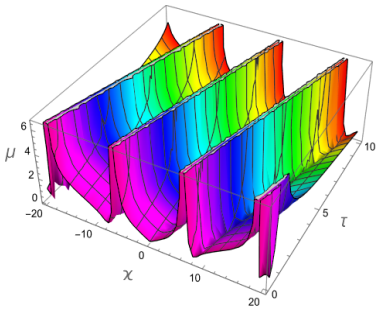

(g) Three-dimensional plot at $\sigma_1 = 0.125$, $\sigma_2 = 0.08$, $\sigma_3 = 0.08$, $\omega = 1.45$, and $\lambda = 1$.

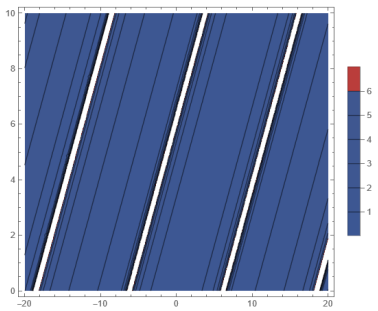

(h) Contour plot at $\sigma_1 = 0.125$, $\sigma_2 = 0.08$, $\sigma_3 = 0.08$, $\omega = 1.45$, and $\lambda = 1$.

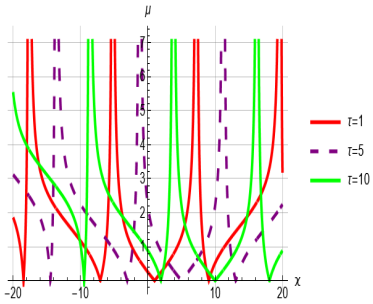

(i) Influence of time on the propagation of waves at $\sigma_1 = 0.125$, $\sigma_2 = 0.08$, $\sigma_3 = 0.08$, $\omega = 1.45$, and $\lambda = 1$.

Figure 3. Dynamic propagation of the soliton solution $\mu_{15}(\varkappa, \tau)$.

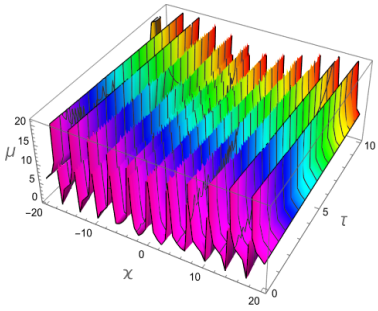

(a) Three-dimensional plot at $\sigma_1 = 0.01$, $\sigma_2 = 0.01$, $\sigma_3 = 1.15$, $\omega = 1.19$, and $\lambda = 0.1$.

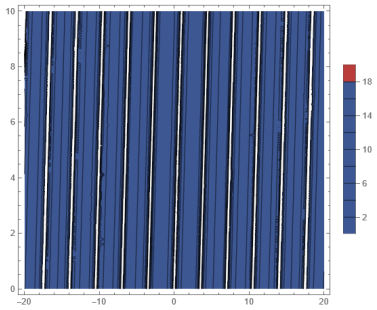

(b) Contour plot at $\sigma_1 = 0.01$, $\sigma_2 = 0.01$, $\sigma_3 = 1.15$, $\omega = 1.19$, and $\lambda = 0.1$.

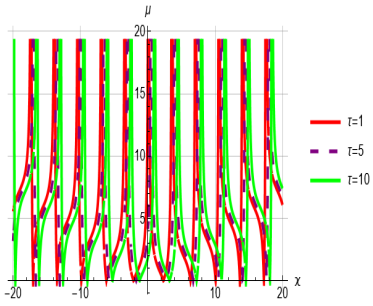

(c) Influence of time on the propagation of waves at $\sigma_1 = 0.01$, $\sigma_2 = 0.01$, $\sigma_3 = 1.15$, $\omega = 1.19$, and $\lambda = 0.1$.

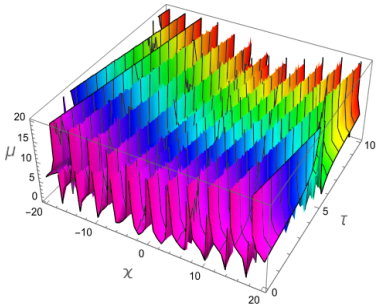

(d) Three-dimensional plot at $\sigma_1 = 0.01$, $\sigma_2 = 0.01$, $\sigma_3 = 1.15$, $\omega = 1.19$, and $\lambda = 0.5$.

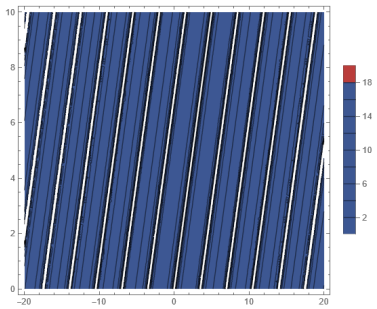

(e) Contour plot at $\sigma_1 = 0.01$, $\sigma_2 = 0.01$, $\sigma_3 = 1.15$, $\omega = 1.19$, and $\lambda = 0.5$.

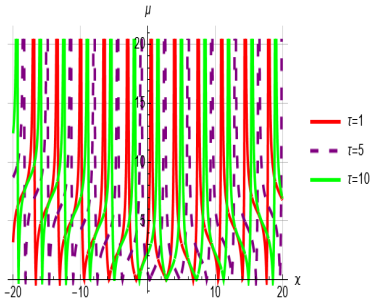

(f) Influence of time on the propagation of waves at $\sigma_1 = 0.01$, $\sigma_2 = 0.01$, $\sigma_3 = 1.15$, $\omega = 1.19$, and $\lambda = 0.5$.

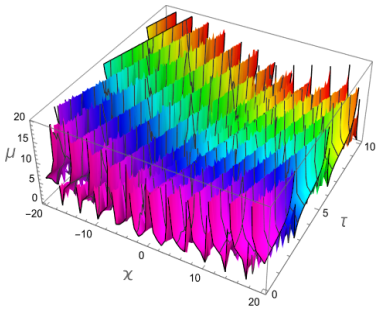

(g) Three-dimensional plot at $\sigma_1 = 0.01$, $\sigma_2 = 0.01$, $\sigma_3 = 1.15$, $\omega = 1.19$, and $\lambda = 1$.

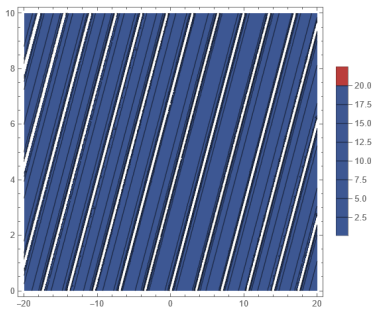

(h) Contour plot at $\sigma_1 = 0.01$, $\sigma_2 = 0.01$, $\sigma_3 = 1.15$, $\omega = 1.19$, and $\lambda = 1$.

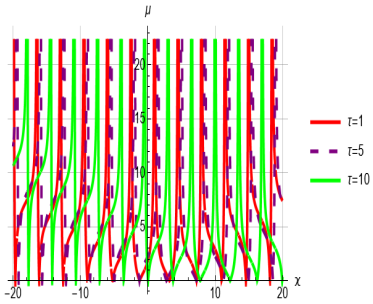

(i) Influence of time on the propagation of waves at $\sigma_1 = 0.01$, $\sigma_2 = 0.01$, $\sigma_3 = 1.15$, $\omega = 1.19$, and $\lambda = 1$.

Figure 4. Dynamic propagation of the soliton solution $\mu_{16}(\varkappa, \tau)$.

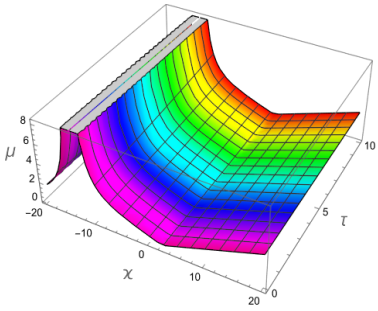

(a) Three-dimensional plot at $\sigma_1 = 0.01$, $\sigma_2 = 0.09$, $\sigma_3 = 1.5$, $\omega = 0.15$, $\rho = 0.8$, and $\lambda = 0.1$.

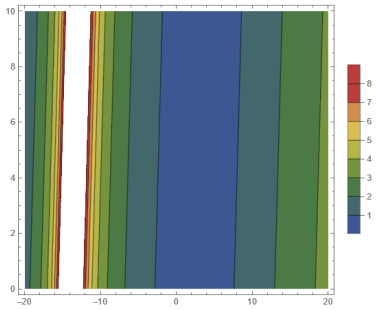

(b) Contour plot at $\sigma_1 = 0.01$, $\sigma_2 = 0.09$, $\sigma_3 = 1.5$, $\omega = 0.15$, $\rho = 0.8$, and $\lambda = 0.1$.

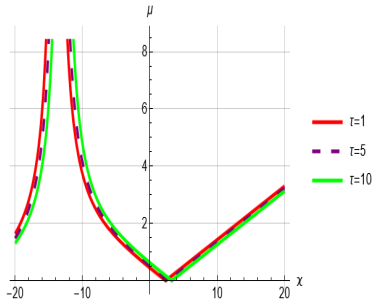

(c) Influence of time on the propagation of waves at $\sigma_1 = 0.01$, $\sigma_2 = 0.09$, $\sigma_3 = 1.5$, $\omega = 0.15$, $\rho = 0.8$, and $\lambda = 0.1$.

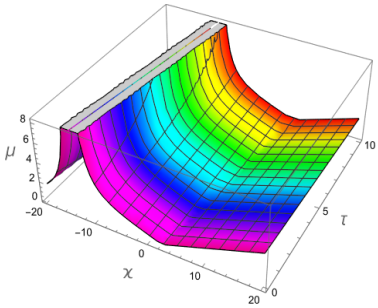

(d) Three-dimensional plot at $\sigma_1 = 0.01$, $\sigma_2 = 0.09$, $\sigma_3 = 1.5$, $\omega = 0.15$, $\rho = 0.8$, and $\lambda = 0.5$.

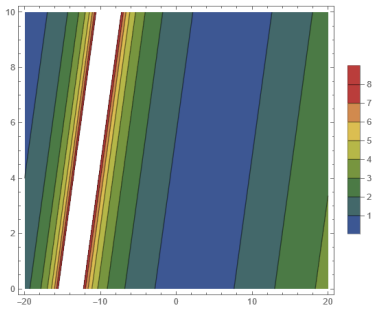

(e) Contour plot at $\sigma_1 = 0.01$, $\sigma_2 = 0.09$, $\sigma_3 = 1.5$, $\omega = 0.15$, $\rho = 0.8$, and $\lambda = 0.5$.

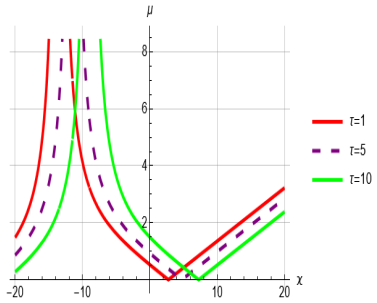

(f) Influence of time on the propagation of waves at $\sigma_1 = 0.01$, $\sigma_2 = 0.09$, $\sigma_3 = 1.5$, $\omega = 0.15$, $\rho = 0.8$, and $\lambda = 0.5$.

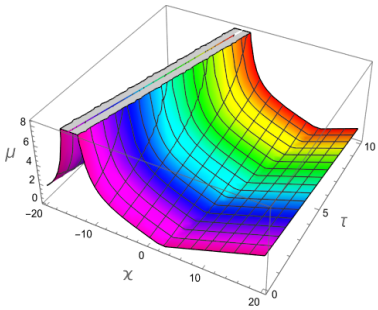

(g) Three-dimensional plot at $\sigma_1 = 0.01$, $\sigma_2 = 0.09$, $\sigma_3 = 1.5$, $\omega = 0.15$, $\rho = 0.8$, and $\lambda = 1$.

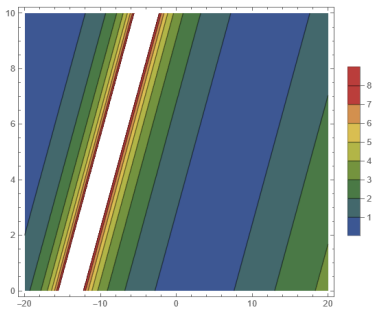

(h) Contour plot at $\sigma_1 = 0.01$, $\sigma_2 = 0.09$, $\sigma_3 = 1.5$, $\omega = 0.15$, $\rho = 0.8$, and $\lambda = 1$.

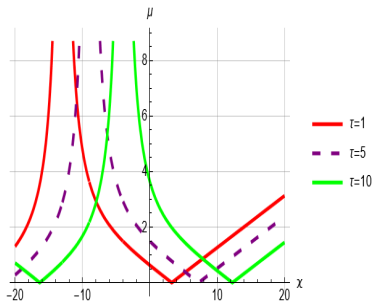

(i) Influence of time on the propagation of waves at $\sigma_1 = 0.01$, $\sigma_2 = 0.09$, $\sigma_3 = 1.5$, $\omega = 0.15$, $\rho = 0.8$, and $\lambda = 1$.

Figure 5. Dynamic propagation of the soliton solution $\mu_{21}(\varkappa, \tau)$.

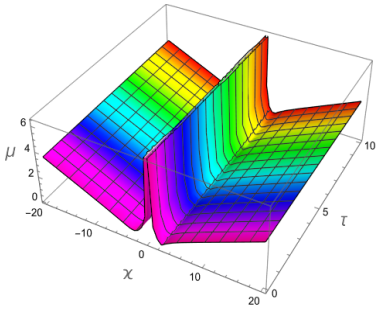

(a) Three-dimensional plot at $\sigma_1 = 0.01$, $\sigma_2 = 0.09$, $\sigma_3 = 1.5$, $\omega = 0.15$, $\rho = 0.08$, and $\lambda = 0.1$.

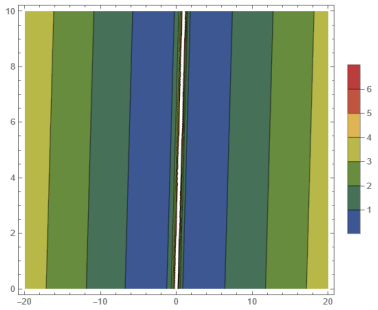

(b) Contour plot at $\sigma_1 = 0.01$, $\sigma_2 = 0.09$, $\sigma_3 = 1.5$, $\omega = 0.15$, $\rho = 0.08$, and $\lambda = 0.1$.

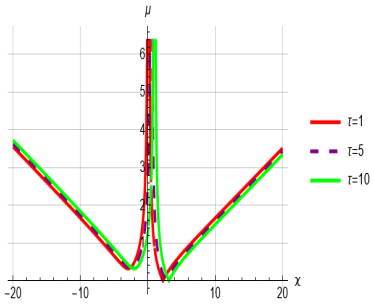

(c) Influence of time on the propagation of waves at $\sigma_1 = 0.01$, $\sigma_2 = 0.09$, $\sigma_3 = 1.5$, $\omega = 0.15$, $\rho = 0.08$, and $\lambda = 0.1$.

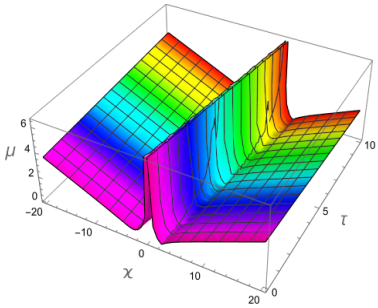

(d) Three-dimensional plot at $\sigma_1 = 0.01$, $\sigma_2 = 0.09$, $\sigma_3 = 1.5$, $\omega = 0.15$, $\rho = 0.08$, and $\lambda = 0.5$.

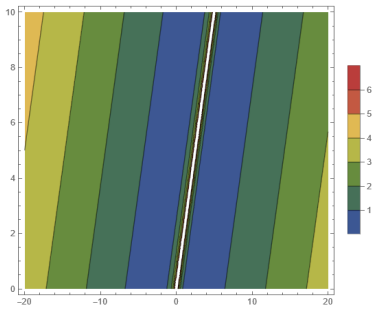

(e) Contour plot at $\sigma_1 = 0.01$, $\sigma_2 = 0.09$, $\sigma_3 = 1.5$, $\omega = 0.15$, $\rho = 0.08$, and $\lambda = 0.5$.

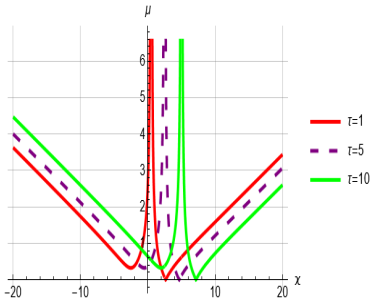

(f) Influence of time on the propagation of waves at $\sigma_1 = 0.01$, $\sigma_2 = 0.09$, $\sigma_3 = 1.5$, $\omega = 0.15$, $\rho = 0.08$, and $\lambda = 0.5$.

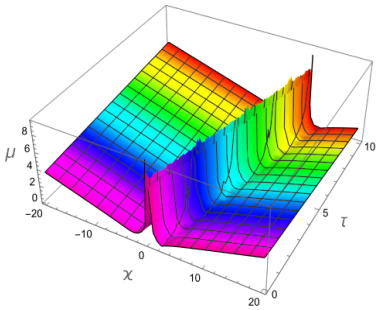

(g) Three-dimensional plot at $\sigma_1 = 0.01$, $\sigma_2 = 0.09$, $\sigma_3 = 1.5$, $\omega = 0.15$, $\rho = 0.08$, and $\lambda = 1$.

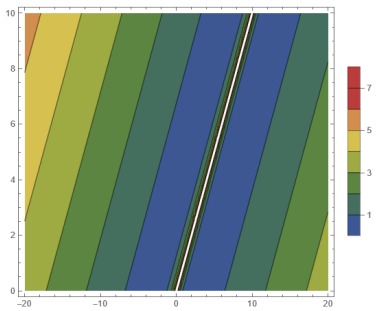

(h) Contour plot at $\sigma_1 = 0.01$, $\sigma_2 = 0.09$, $\sigma_3 = 1.5$, $\omega = 0.15$, $\rho = 0.08$, and $\lambda = 1$.

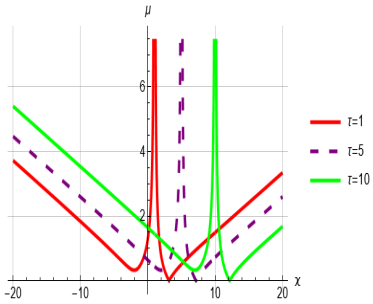

(i) Influence of time on the propagation of waves at $\sigma_1 = 0.01$, $\sigma_2 = 0.09$, $\sigma_3 = 1.5$, $\omega = 0.15$, $\rho = 0.08$, and $\lambda = 1$.

Figure 6. Dynamic propagation of the soliton solution $\mu_{23}(\varkappa, \tau)$.

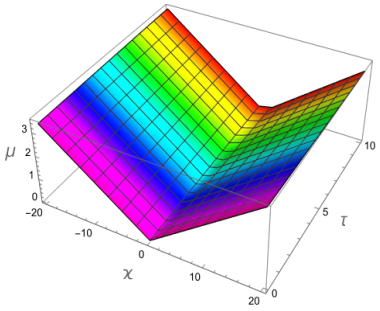

(a) Three-dimensional plot at $\varpi_1 = 0.01$, $\eta_0 = 0.5$, $\varpi_2 = 1.2$, $\omega = 0.01$, and $\lambda = 0.1$.

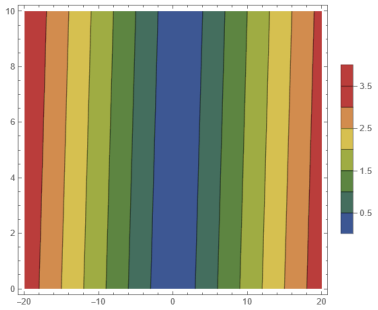

(b) Contour plot at $\varpi_1 = 0.01$, $\eta_0 = 0.5$, $\varpi_2 = 1.2$, $\omega = 0.01$, and $\lambda = 0.1$.

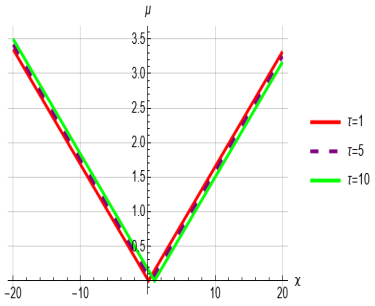

(c) Influence of time on the propagation of waves at $\varpi_1 = 0.01$, $\eta_0 = 0.5$, $\varpi_2 = 1.2$, $\omega = 0.01$, and $\lambda = 0.1$.

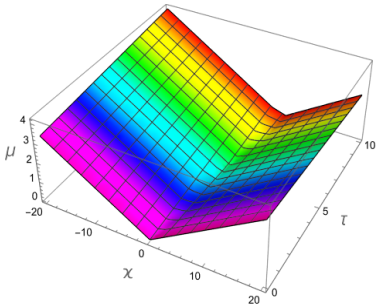

(d) Three-dimensional plot at $\varpi_1 = 0.01$, $\eta_0 = 0.5$, $\varpi_2 = 1.2$, $\omega = 0.01$, and $\lambda = 0.5$.

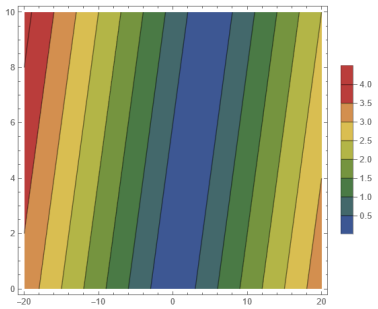

(e) Contour plot at $\varpi_1 = 0.01$, $\eta_0 = 0.5$, $\varpi_2 = 1.2$, $\omega = 0.01$, and $\lambda = 0.5$.

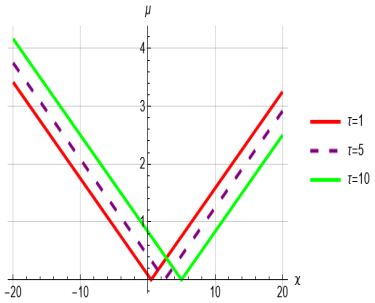

(f) Influence of time on the propagation of waves at $\varpi_1 = 0.01$, $\eta_0 = 0.5$, $\varpi_2 = 1.2$, $\omega = 0.01$, and $\lambda = 0.5$.

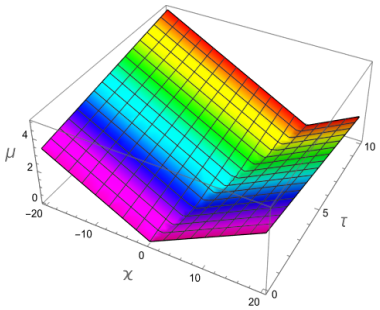

(g) Three-dimensional plot at $\varpi_1 = 0.01$, $\eta_0 = 0.5$, $\varpi_2 = 1.2$, $\omega = 0.01$, and $\lambda = 1$.

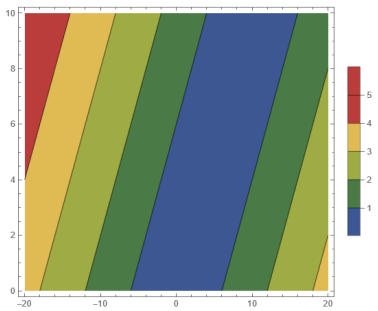

(h) Contour plot at $\varpi_1 = 0.01$, $\eta_0 = 0.5$, $\varpi_2 = 1.2$, $\omega = 0.01$, and $\lambda = 1$.

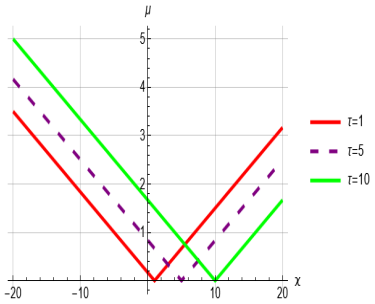

(i) Influence of time on the propagation of waves at $\varpi_1 = 0.01$, $\eta_0 = 0.5$, $\varpi_2 = 1.2$, $\omega = 0.01$, and $\lambda = 1$.

Figure 7. Dynamic propagation of the soliton solution $\mu_{F1}(\varkappa, \tau)$.

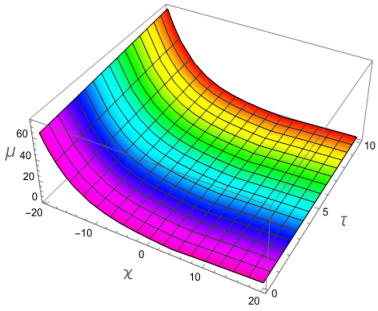

(a) Three-dimensional plot at $\varpi_1 = 0.01$, $\eta_0 = 0.5$, $\varpi_2 = 0.2$, $\omega = 0.9$, and $\lambda = 0.1$.

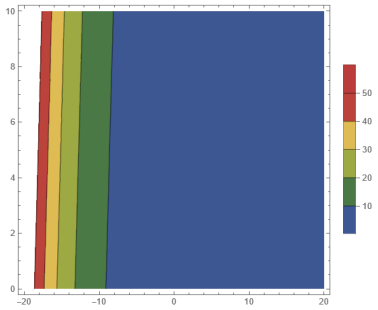

(b) Contour plot at $\varpi_1 = 0.01$, $\eta_0 = 0.5$, $\varpi_2 = 0.2$, $\omega = 0.9$, and $\lambda = 0.1$.

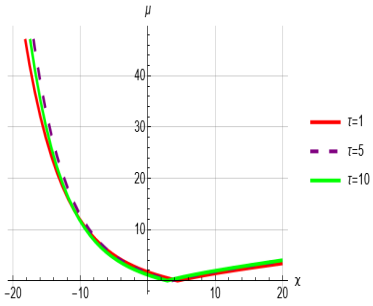

(c) Influence of time on the propagation of waves at $\varpi_1 = 0.01$, $\eta_0 = 0.5$, $\varpi_2 = 0.2$, $\omega = 0.9$, and $\lambda = 0.1$.

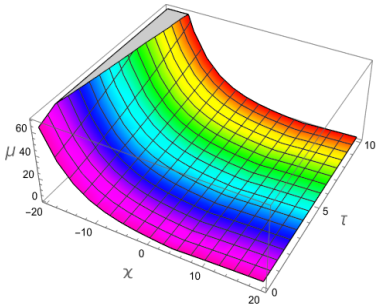

(d) Three-dimensional plot at $\varpi_1 = 0.01$, $\eta_0 = 0.5$, $\varpi_2 = 0.2$, $\omega = 0.9$, and $\lambda = 0.5$.

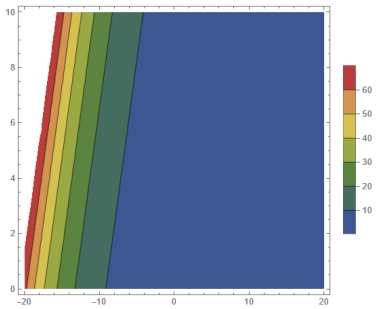

(e) Contour plot at $\varpi_1 = 0.01$, $\eta_0 = 0.5$, $\varpi_2 = 0.2$, $\omega = 0.9$, and $\lambda = 0.5$.

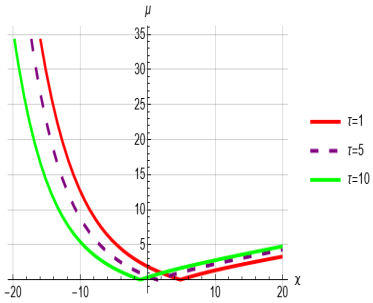

(f) Influence of time on the propagation of waves at $\varpi_1 = 0.01$, $\eta_0 = 0.5$, $\varpi_2 = 0.2$, $\omega = 0.9$, and $\lambda = 0.5$.

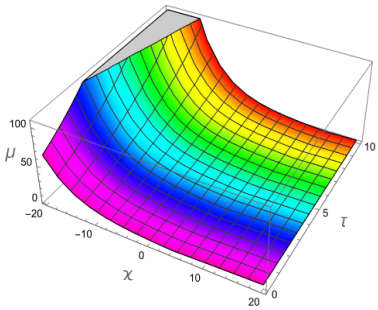

(g) Three-dimensional plot at $\varpi_1 = 0.01$, $\eta_0 = 0.5$, $\varpi_2 = 0.2$, $\omega = 0.9$, and $\lambda = 1$.

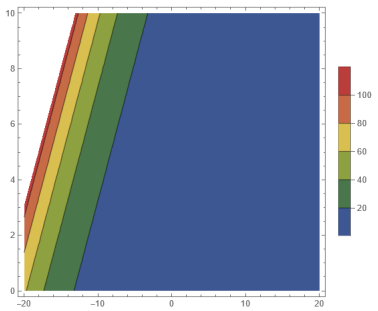

(h) Contour plot at $\varpi_1 = 0.01$, $\eta_0 = 0.5$, $\varpi_2 = 0.2$, $\omega = 0.9$, and $\lambda = 1$.

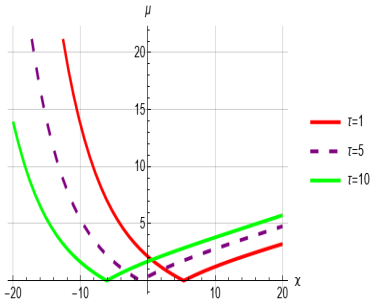

(i) Influence of time on the propagation of waves at $\varpi_1 = 0.01$, $\eta_0 = 0.5$, $\varpi_2 = 0.2$, $\omega = 0.9$, and $\lambda = 1$.

Figure 8. Dynamic propagation of the soliton solution $\mu_{F5}(\varkappa, \tau)$.

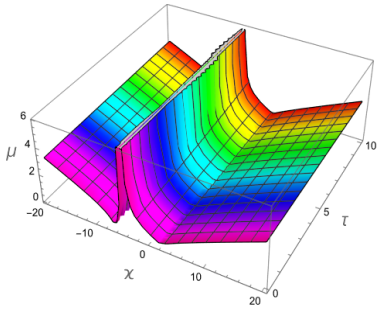

(a) Three-dimensional plot at $\varpi_1 = 0.01$, $\eta_0 = 0.5$, $\varpi_2 = 1.2$, $\omega = 0.1$, and $\lambda = 0.1$.

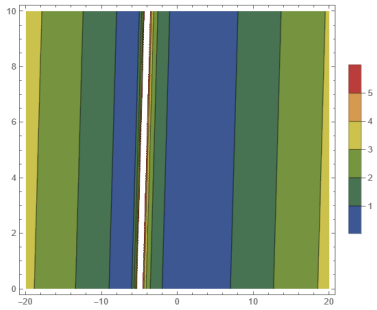

(b) Contour plot at $\varpi_1 = 0.01$, $\eta_0 = 0.5$, $\varpi_2 = 1.2$, $\omega = 0.1$, and $\lambda = 0.1$.

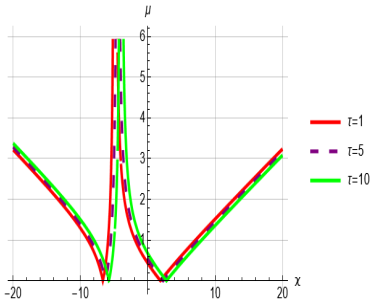

(c) Influence of time on the propagation of waves at $\varpi_1 = 0.01$, $\eta_0 = 0.5$, $\varpi_2 = 1.2$, $\omega = 0.1$, and $\lambda = 0.1$.

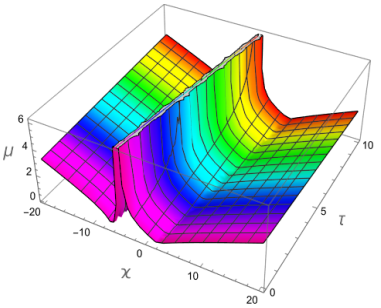

(d) Three-dimensional plot at $\varpi_1 = 0.01$, $\eta_0 = 0.5$, $\varpi_2 = 1.2$, $\omega = 0.1$, and $\lambda = 0.5$.

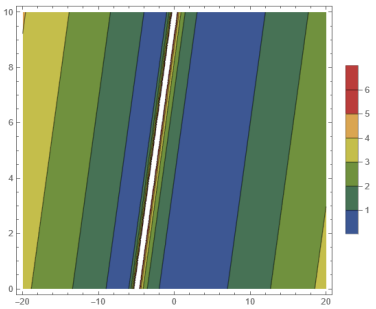

(e) Contour plot at $\varpi_1 = 0.01$, $\eta_0 = 0.5$, $\varpi_2 = 1.2$, $\omega = 0.1$, and $\lambda = 0.5$.

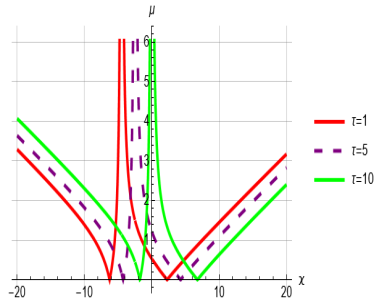

(f) Influence of time on the propagation of waves at $\varpi_1 = 0.01$, $\eta_0 = 0.5$, $\varpi_2 = 1.2$, $\omega = 0.1$, and $\lambda = 0.5$.

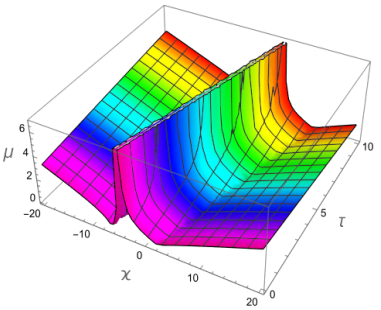

(g) Three-dimensional plot at $\varpi_1 = 0.01$, $\eta_0 = 0.5$, $\varpi_2 = 1.2$, $\omega = 0.1$, and $\lambda = 1$.

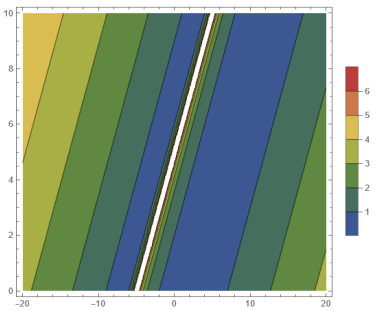

(h) Contour plot at $\varpi_1 = 0.01$, $\eta_0 = 0.5$, $\varpi_2 = 1.2$, $\omega = 0.1$, and $\lambda = 1$.

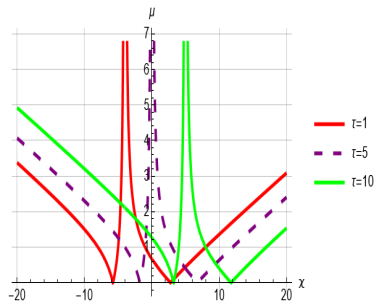

(i) Influence of time on the propagation of waves at $\varpi_1 = 0.01$, $\eta_0 = 0.5$, $\varpi_2 = 1.2$, $\omega = 0.1$, and $\lambda = 1$.

Figure 9. Dynamic propagation of the soliton solution $\mu_{F8}(\varkappa, \tau)$.

5. Conclusions

The Kumar–Malik method and the extended hyperbolic function method have been successfully applied to construct the numerous analytical exact soliton solutions for the nonlinear Kairat-II equation that explain important scientific and engineering phenomena. The solutions encompass a broad

spectrum of soliton types, including bright, dark, singular, periodic, exponential forms, and Jacobi elliptic function solutions with an elliptic modulus. The diversity of these solutions reveals rich patterns, such as exponential, plane wave, and shock wave structures, which enhance the understanding of soliton's dynamics in nonlinear optical systems. The graphical representations, including 2D, 3D, and contour plots, provide valuable insights into key soliton behaviors, highlighting the impact of parameters, particularly the wave number, on solitons' amplitude, motion, and singularity. These results underline the importance of tunability in shaping solitons' characteristics, offering a powerful tool for controlling solitons' properties in nonlinear media. The demonstrated effectiveness of the applied methods in generating exact solutions to the Kairat-II equation lays a solid foundation for further research on soliton-based technologies, with potential applications in fields such as optical communications and materials science. The obtained solutions show that these analytical techniques can be used for other dynamic models for analytical study. However, the Kumar–Malik method, while effective for certain soliton solutions, is limited by its applicability to equations that can be transformed into a suitable form, which excludes some nonlinear equations. It also becomes computationally intensive for higher-order equations, requiring complex algebraic manipulations. Moreover, the solutions obtained may be difficult to interpret or apply due to their complexity. Similarly, the extended hyperbolic function method is most useful for equations with hyperbolic nonlinearities, limiting its general applicability. The solutions can be complex, making analysis challenging; in some cases, the method may fail to provide real solutions. Additionally, the success of both methods depends on correct transformations, and improper choices may lead to failure in obtaining meaningful solutions. In the future, this study could be extended to the fractional domain, as fractional derivatives provide a more accurate representation of memory and hereditary effects in complex systems. Fractional extensions of the K-II equation could offer deeper insights into soliton dynamics in heterogeneous and anomalous media, making them highly relevant for applications in optical fibers, plasma physics, and biological systems. Furthermore, the proposed approach can be further expanded to different classes of fractional differential equations in future work; more appealingly, the meanings of the obtained solutions in various practical applications can be studied, which provides a valuable method for researchers in fractional calculus and nonlinear dynamics.

Authors contributions

Abdul Mateen: Conceptualization, methodology, software, validation, investigation, writing-original draft preparation, writing-review and editing, visualization; Ghulam Hussain Tipu: Methodology, validation, investigation, writing-review and editing, visualization; Loredana Ciurdariu: Validation, investigation, visualization; Fengping Yao: Validation, investigation, visualization, supervision. All authors have read and agreed to the final version of the manuscript.

Use of Generative-AI tools declaration

The authors declare they have not used artificial intelligence (AI) tools in the creation of this article.

Conflict of interest

The authors declare no conflict of interest.

References

1. S. Dong, Z. Z. Lan, B. Gao, Y. Shen, Bäcklund transformation and multi-soliton solutions for the discrete Korteweg-de Vries equation, *Appl. Math. Lett.*, **125** (2022), 107747. https://doi.org/10.1016/j.aml.2021.107747
2. X. Liu, H. Zhang, W. Liu, The dynamic characteristics of pure-quartic solitons and soliton molecules, *Appl. Math. Model.*, **102** (2022), 305–312. https://doi.org/10.1016/j.apm.2021.09.042
3. L. Akinyemi, Shallow ocean soliton and localized waves in extended (2+1)-dimensional non-linear evolution equations, *Phys. Lett. A*, **463** (2023), 128668. https://doi.org/10.1016/j.physleta.2023.128668
4. R. F. Zhang, M. C. Li, J. Y. Gan, Q. Li, Z. Z. Lan, Novel trial functions and rogue waves of generalized breaking soliton equation via bilinear neural network method, *Chaos Soliton. Fract.*, **154** (2022), 111692. https://doi.org/10.1016/j.chaos.2021.111692
5. C. Kumar, A. Prakash, Non-linear interaction among second mode resonance waves in high-speed boundary layers using the method of multiple scales, *Phys. Fluids*, **34** (2022), 014107. https://doi.org/10.1063/5.0078099
6. C. Zhang, Z. Shi, Non-linear wave interactions in a transitional hypersonic boundary layer, *Phys. Fluids*, **34** (2022), 114106. https://doi.org/10.1063/5.0120425
7. G. Tao, J. Sabi'u, S. Nestor, R. M. E. Shiekh, L. Akinyemi, E. A. Zo'bi, et al., Dynamics of a new class of solitary wave structures in telecommunications systems via [2+1]-dimensional non-linear transmission line, *Mod. Phys. Lett. B*, **36** (2022), 2150596. https://doi.org/10.1142/S0217984921505965
8. M. A. Isah, M. A. Külahcı, A study on null cartan curve in Minkowski 3-space, *Appl. Math. Nonlin. Sci.*, **5** (2020), 413–424. https://doi.org/10.2478/amns.2020.1.00039
9. M. A. Isah, M. A. Külahçı, Special curves according to bishop frame in Minkowski 3-space, *Appl. Math. Nonlin. Sci.*, **5** (2020), 237–248. https://doi.org/10.2478/amns.2020.1.00021
10. S. Kumar, B. Mohan, R. Kumar, Lump, soliton, and interaction solutions to a generalized two-mode higher-order non-linear evolution equation in plasma physics, *Nonlinear Dynam.*, **110** (2022), 693–704. https://doi.org/10.1007/s11071-022-07647-5
11. U. Younas, T. A. Sulaiman, J. Ren, On the study of optical soliton solutions to the three-component coupled non-linear Schrödinger equation: Applications in fiber optics, *Opt. Quant. Electron.*, **55** (2023), 72. https://doi.org/10.1007/s11082-022-04254-x
12. U. Younas, T. A. Sulaiman, J. Ren, Diversity of optical soliton structures in the spinor Bose-Einstein condensate modeled by three-component Gross-Pitaevskii system, *Int. J. Mod. Phys. B*, **37** (2023), 2350004. https://doi.org/10.1142/S0217979223500042
13. S. Kumar, A. Kumar, Abundant closed-form wave solutions and dynamical structures of soliton solutions to the [3+1]-dimensional BLMP equation in mathematical physics, *J. Ocean Eng. Sci.*, **7** (2022), 178–187. https://doi.org/10.1016/j.joes.2021.08.001

14. G. H. Tipu, W. A. Faridi, Z. Myrzakulova, R. Myrzakulov, S. A. AlQahtani, N. F. AlQahtani, et al., On optical soliton wave solutions of non-linear Kairat-X equation via new extended direct algebraic method, *Opt. Quant. Electron.*, **56** (2024), 655. https://doi.org/10.1007/s11082-024-06369-9
15. Y. Li, S. F. Tian, J. J. Yang, Riemann-Hilbert problem and interactions of solitons in the component nonlinear Schrödinger equations, *Stud. Appl. Math.*, **148** (2022), 577–605. https://doi.org/10.1111/sapm.12450
16. M. I. Asjad, H. U. Rehman, Z. Ishfaq, J. Awrejcewicz, A. Akgül, M. B. Riaz, On soliton solutions of perturbed Boussinesq and KdV-Caudery-Dodd-Gibbon equations, *Coatings*, **11** (2021), 1429. https://doi.org/10.3390/coatings11111429
17. F. Tchier, A. Yusuf, A. I. Aliyu, M. Inc, Soliton solutions and conservation laws for lossy nonlinear transmission line equation, *Superlattice. Microst.*, **107** (2017), 320. https://doi.org/10.1016/j.spmi.2017.04.003
18. J. Manafian, M. Lakestani, A new analytical approach to solve some of the fractional-order partial differential equations, *Indian J. Phys.*, **91** (2017), 243. https://doi.org/10.1007/s12648-016-0912-z
19. W. A. Faridi, M. A. Bakar, Z. Myrzakulova, R. Myrzakulov, A. Akgül, S. M. E. Din, The formation of solitary wave solutions and their propagation for Kuralay equation, *Results Phys.*, **52** (2023), 106774. https://doi.org/10.1016/j.rinp.2023.106774
20. M. Mirzazadeh, M. Eslami, Exact multisoliton solutions of nonlinear Klein-Gordon equation in [1+2]-dimensions, *Eur. Phys. J. Plus*, **128** (2013), 132. https://doi.org/10.1140/epjp/i2013-13132-y
21. W. X. Ma, A combined Kaup-Newell type integrable Hamiltonian hierarchy with four potentials and a hereditary recursion operator, *Discrete Cont. Dyn.-S*, **18** (2024), 931–941. https://doi.org/10.3934/dcdss.2024117
22. M. Gürses, A. Pekcan, Nonlocal nonlinear Schrödinger equations and their soliton solutions, *J. Math. Phys.*, **59** (2018), 051501. https://doi.org/10.1063/1.4997835
23. W. X. Ma, Type (λ^*, λ) reduced nonlocal integrable AKNS equations and their soliton solutions, *Appl. Numer. Math.*, **199** (2024), 105. https://doi.org/10.1016/j.apnum.2022.12.007
24. W. A. Faridi, A. M. Wazwaz, A. M. Mostafa, R. Myrzakulov, Z. Umurzakhova, The Lie point symmetry criteria and formation of exact analytical solutions for Kairat-II equation: Paul-Painlevé approach, *Chaos Soliton. Fract.*, **182** (2024), 114745. https://doi.org/10.1016/j.chaos.2024.114745
25. W. X. Ma, The algebraic structure of zero curvature representations and application to coupled KdV systems, *J. Phys. A-Math. Gen.*, **26** (1993), 2573. https://doi.org/10.1088/0305-4470/26/11/009
26. Z. Z. Lan, Multi-soliton solutions, breather-like and bound-state solitons for complex modified Korteweg-de Vries equation in optical fibers, *Chinese Phys. B*, **33** (2024), 060201. https://doi.org/10.1088/1674-1056/ad39d7
27. N. Nasreen, A. R. Seadawy, D. Lu, M. Arshad, Optical fibers to model pulses of ultrashort via generalized third-order non-linear Schrödinger equation by using extended and modified rational expansion method, *J. Nonlinear Opt. Phys.*, **33** (2023), 2350058. https://doi.org/10.1142/S0218863523500583
28. N. Nasreen, D. Lu, Z. Zhang, A. Akgül, U. Younas, S. Nasreen, et al., Propagation of optical pulses in fiber optics modeled by coupled space-time fractional dynamical system, *Alex. Eng. J.*, **73** (2023), 173–187. https://doi.org/10.1016/j.aej.2023.04.046

29. M. B. Almatrafi, Solitary wave solutions to a fractional model using the improved modified extended tanh-function method, *Fractal Fract.*, **7** (2023), 252. https://doi.org/10.3390/fractalfract7030252

30. H. F. Ismael, U. Younas, T. A. Sulaiman, N. Nasreen, N. A. Shah, M. R. Ali, Non classical interaction aspects to a non-linear physical model, *Results Phys.*, **49** (2023), 106520. https://doi.org/10.1016/j.rinp.2023.106520

31. S. Samir, E. Salah, E. A. E. Dahab, H. M. Ahmed, M. Ammar, W. Alexan, et al., Unraveling solitons dynamics in system of dispersive NLSE with Kudryashov's law of nonlinearity using improved modified extended tanh function method, *Alex. Eng. J.*, **91** (2024), 419–428. https://doi.org/10.1016/j.aej.2024.02.020

32. T. Ma, S. Wang, *Bifurcation theory and applications*, World Scientific, **53** (2005).

33. W. A. Faridi, M. Iqbal, M. B. Riaz, S. A. AlQahtani, A. M. Wazwaz, The fractional soliton solutions of dynamical system arising in plasma physics: The comparative analysis, *Alex. Eng. J.*, **95** (2024), 247. https://doi.org/10.1016/j.aej.2024.03.061

34. R. Ali, T. Xie, M. Awais, R. Babar, Deflection angle and shadow evolution from charged torus-like black hole under the effect of non-magnetic plasma and non-plasma medium, *Int. J. Geom. Methods M.*, **21** (2024), 2450180. https://doi.org/10.1142/S0219887824501809

35. J. Y. Yang, W. X. Ma, Four-component Liouville integrable models and their bi-Hamiltonian formulations, *Rom. J. Phys.*, **69** (2024), 10.

36. W. X. Ma, Integrable couplings and two-dimensional unital algebras, *Axioms*, **13** (2024), 481. https://doi.org/10.3390/axioms13070481

37. A. Jhangeer, Beenish, Dynamics and wave analysis in longitudinal motion of elastic bars or fluids, *Ain Shams Eng. J.*, **15** (2024), 102907. https://doi.org/10.1016/j.asej.2024.102907

38. A. Jhangeer, A. R. Ansari, M. Imran, Beenish, M. B. Riaz, Lie symmetry analysis, and traveling wave patterns arising in the model of transmission lines, *AIMS Math.*, **9** (2024), 18013. https://doi.org/10.3934/math.2024878

39. L. Yang, H. Huang, Z. Xi, L. Zheng, S. Xu, G. Tian, et al., Simultaneously achieving giant piezoelectricity and record coercive field enhancement in relaxor-based ferroelectric crystals, *Nat. Commun.*, **13** (2022), 2444. https://doi.org/10.1038/s41467-022-29962-6

40. Y. M. Chu, S. Arshed, M. Sadaf, G. Akram, M. Maqbool, Solitary wave dynamics of thin-film ferroelectric material equation, *Results Phys.*, **45** (2023), 106201. https://doi.org/10.1016/j.rinp.2022.106201

41. X. Wang, H. Ehsan, M. Abbas, G. Akram, M. Sadaf, T. Abdeljawad, Analytical solitary wave solutions of a time-fractional thin-film ferroelectric material equation involving beta-derivative using modified auxiliary equation method, *Results Phys.*, **48** (2023), 106411. https://doi.org/10.1016/j.rinp.2023.106411

42. A. Souleymanou, K. K. Ali, H. Rezazadeh, M. Eslami, M. Mirzazadeh, A. Korkmaz, The propagation of waves in thin-film ferroelectric materials, *Pramana*, **93** (2019), 27. https://doi.org/10.1007/s12043-019-1774-7

43. W. A. Faridi, M. A. Bakar, A. Akgül, M. Abd E. Rahman, S. M. El Din, Exact fractional soliton solutions of thin-film ferroelectric material equation by analytical approaches, *Alex. Eng. J.*, **78** (2023), 483. https://doi.org/10.1016/j.aej.2023.07.049
44. Z. Myrzakulova, S. Manukure, R. Myrzakulov, G. Nugmanova, Integrability, geometry and wave solutions of some Kairat equations, *arXiv Preprint*, 2023. https://doi.org/10.48550/arXiv.2307.00027
45. F. N. K. Sağlam, S. Malik, Various traveling wave solutions for (2+1)-dimensional extended Kadomtsev-Petviashvili equation using a newly created methodology, *Chaos Soliton. Fract.*, **186** (2024), 115318. https://doi.org/10.1016/j.chaos.2024.115318
46. G. H. Tipu, W. A. Faridi, M. B. Riaz, F. P. Yao, U. Younas, M. Garayev, Chaotic analysis and a damped oscillator solitary wave structures to the generalized reaction Duffing model, *Results Phys.*, **72** (2025), 108203. https://doi.org/10.1016/j.rinp.2025.108203
47. U. Younas, J. Muhammad, D. K. Almutairi, A. Khan, T. Abdeljawad, Analyzing the neural wave structures in the field of neuroscience, *Sci. Rep.*, **15** (2025), 7181. https://doi.org/10.1038/s41598-025-91397-y
48. L. Borcea, J. Garnier, Enhanced wave transmission in random media with mirror symmetry, *P. Roy. Soc. A*, **480** (2024), 20240073. https://doi.org/10.1098/rspa.2024.0073

AIMS Press